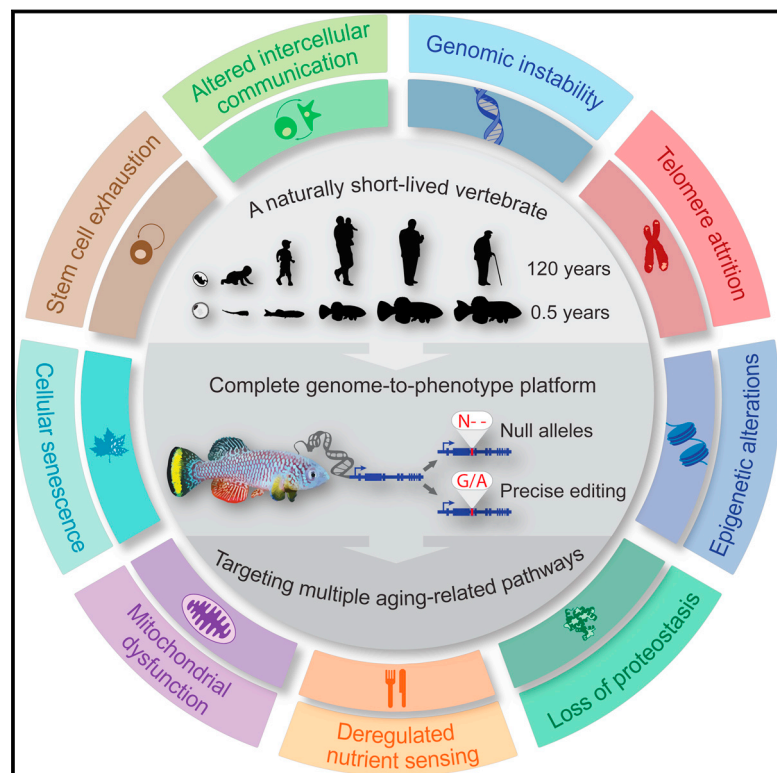# A Platform for Rapid Exploration of Aging and Diseases in a Naturally Short-Lived Vertebrate

Graphical Abstract

Authors

Itamar Harel, Bérénice A. Benayoun, ..., Steven E. Artandi, Anne Brunet

Correspondence

abrunet1@stanford.edu

In Brief

Aging is the number one risk factor for many human pathologies, yet it is challenging to study as existing vertebrate models are relatively long lived. The development of an integrative genome-to-phenotype platform in a naturally short-lived vertebrate, the African turquoise killifish, opens the door to high-throughput in vivo modeling of vertebrate aging and complex human diseases.

Highlights

- The turquoise killifish is the shortest-lived vertebrate species bred in the lab

- A complete genome-to-phenotype platform for this emerging model

- Telomerase-deficient fish display the fastest onset of related human pathologies

- A resource of targeted aging- and disease-related genes and available fish lines

Accession Numbers

JNBZ00000000
SRP041421
SRP045718

CrossMark

CellPress

A Platform for Rapid Exploration of Aging and Diseases in a Naturally Short-Lived Vertebrate

Itamar Harel,[1] Bérénice A. Benayoun,[1] Ben Machado,[1] Param Priya Singh,[1] Chi-Kuo Hu,[1] Matthew F. Pech,[2,3] Dario Riccardo Valenzano,[1,5] Elisa Zhang,[1] Sabrina C. Sharp,[1] Steven E. Artandi,[2,3,4] and Anne Brunet[1,4,*]

[1]Department of Genetics, Stanford University, Stanford, CA 94305, USA
[2]Department of Medicine, Stanford University School of Medicine, Stanford, CA 94305, USA
[3]Biochemistry Department, Stanford University School of Medicine, Stanford, CA 94305, USA
[4]Glenn Laboratories for the Biology of Aging at Stanford, Stanford, CA 94305, USA
[5]Present address: Max Planck Institute for Biology of Ageing, Cologne 50931, Germany
*Correspondence: abrunet1@stanford.edu
http://dx.doi.org/10.1016/j.cell.2015.01.038

SUMMARY

Aging is a complex process that affects multiple organs. Modeling aging and age-related diseases in the lab is challenging because classical vertebrate models have relatively long lifespans. Here, we develop the first platform for rapid exploration of age-dependent traits and diseases in vertebrates, using the naturally short-lived African turquoise killifish. We provide an integrative genomic and genome-editing toolkit in this organism using our de-novo-assembled genome and the CRISPR/Cas9 technology. We mutate many genes encompassing the hallmarks of aging, and for a subset, we produce stable lines within 2–3 months. As a proof of principle, we show that fish deficient for the protein subunit of telomerase exhibit the fastest onset of telomere-related pathologies among vertebrates. We further demonstrate the feasibility of creating specific genetic variants. This genome-to-phenotype platform represents a unique resource for studying vertebrate aging and disease in a high-throughput manner and for investigating candidates arising from human genome-wide studies.

INTRODUCTION

Aging is the number one risk factor for many human pathologies, including diabetes, cancer, cardiovascular, and neurodegenerative diseases (Niccoli and Partridge, 2012). Thus, delaying aging could help postpone the onset of these devastating ailments and increase healthspan. Because aging affects multiple organs and systems in humans (López-Otín et al., 2013), it is one of the most challenging processes to model in the lab. So far, the study of aging has been dominated by non-vertebrate short-lived model organisms, such as yeast (C. cerevisiae), worm (C. elegans), and fly (D. melanogaster), which has allowed the identification of remarkably conserved aging-related pathways, such as the TOR and Insulin/IGF pathways (Kenyon, 2010). However,

some important aspects of human aging and disease phenotypes cannot be faithfully recapitulated in invertebrate models, as they lack specific organs and systems (e.g., blood, bones, and an adaptive immune system) that are crucial components of human aging and age-related pathologies. Vertebrate model systems, namely the mouse (M. musculus) and zebrafish (D. rerio), have also been exploited to probe genes involved in aging and age-related diseases. However, experimental studies have been hampered by the relatively long lifespan of mice and zebrafish (maximal lifespan of 3–4 and 5 years, respectively [Tacutu et al., 2013]) and high costs of maintenance, especially for mice. Mouse models with accelerated onset of age-associated disease (e.g., neurodegeneration) can partially address this issue (Trancikova et al., 2011), but these models uncouple the disease phenotype from its main risk factor—aging—and they remain expensive to use. Thus, a new vertebrate model is needed to better understand the principles of vertebrate aging and to study age-related diseases in the context of aging.

The African turquoise killifish Nothobranchius furzeri is a naturally short-lived vertebrate that lives in ephemeral water ponds in Zimbabwe and Mozambique (Figure 1A), where water is only present during a brief rainy season. This fish species has likely evolved a compressed life cycle (as short as 30–40 days from egg to egg-laying adult) to adapt to its transient habitat. The turquoise killifish is currently the shortest-lived vertebrate that can be bred in captivity (Genade et al., 2005; Valenzano et al., 2006), with a lifespan of 4–6 months in optimal laboratory conditions (6 to 10 times shorter than the lifespan of mice and zebrafish, respectively). Importantly, despite its short lifespan, this fish recapitulates typical age-dependent phenotypes and pathologies such as decline in fertility, sarcopenia, cognitive decline, and cancerous lesions (Di Cicco et al., 2011; Genade et al., 2005; Valenzano et al., 2006). It also displays a conserved response to environmental stimuli known to affect the aging rate in other species, such as dietary restriction (Terzibasi et al., 2009). These characteristics make this fish an attractive model organism to study vertebrate aging, physiology, and age-dependent diseases throughout organismal lifespan (Di Cicco et al., 2011). Furthermore, the turquoise killifish telomeres are similar in length to those of humans (6–8 kb) (Hartmann et al., 2009), unlike laboratory mouse telomeres, which are
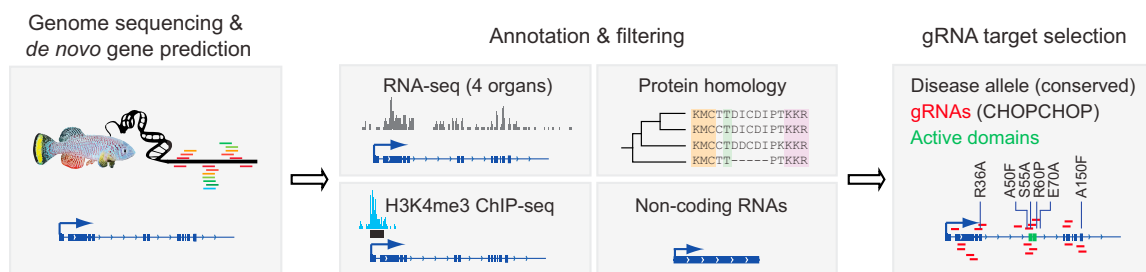
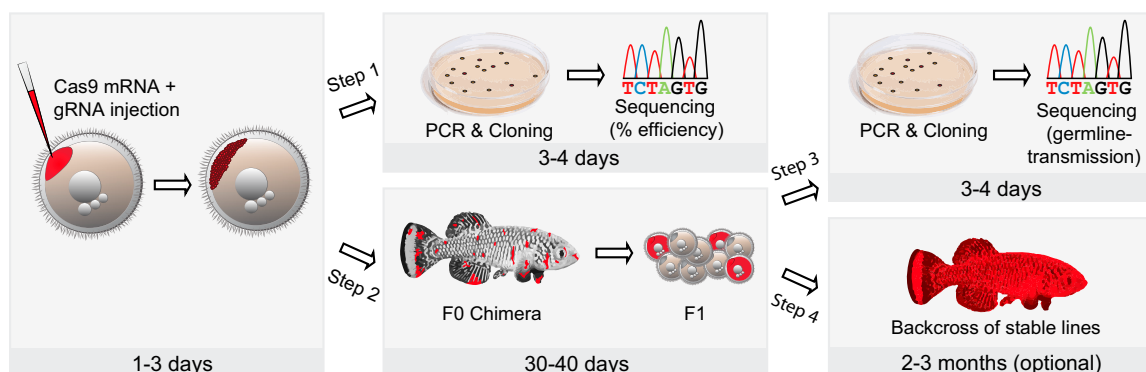**A** Vertebrate and non-vertebrate genetic aging models
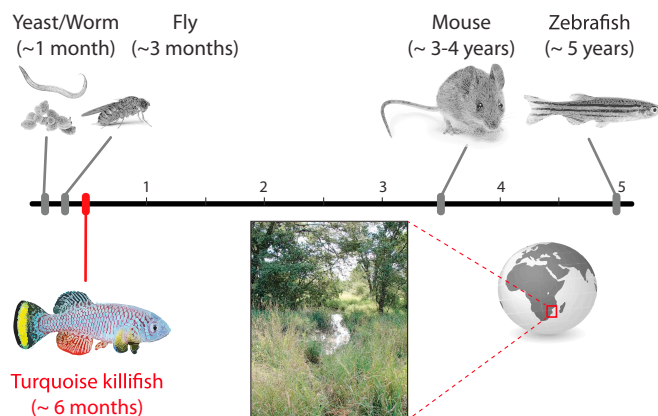
B Targeted genes encompassing the 9 "hallmarks of aging"
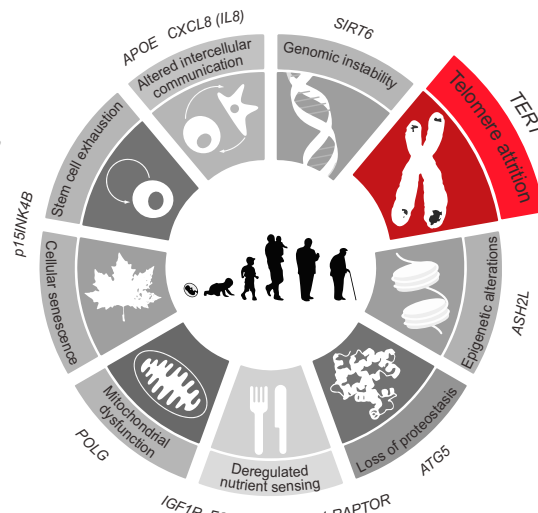
C Genomic pipeline

D Genome-editing pipeline

Figure 1. A Versatile Platform for Rapid Exploration of Aging and Longevity Genes in the Naturally Short-Lived Turquoise Killifish

(A) Lifespan of non-vertebrate and vertebrate model systems widely used for aging and disease research (top), when compared to the lifespan of the turquoise killifish (bottom). The turquoise killifish originates from ephemeral water ponds in Zimbabwe and Mozambique (bottom).

(B) Examples of genes encompassing the hallmarks of human aging (modified with permission from López-Otín et al. [2013]).

(C) Genomic pipeline to generate CRISPR/Cas9 gRNAs in a new model organism using our newly created genomic tools (de-novo-assembled turquoise killifish genome, epigenome, and transcriptome). Gene models and gRNA selection are available via CHOPCHOP.

(D) CRISPR/Cas9 genome-editing pipeline to generate stable mutant fish lines in the turquoise killifish. Overall, the total time for generating a stable mutant line in the lab (i.e., steps 1–4) is about 2–3 months.

very long (50–150 kb) (Lee et al., 1998). Thus, findings from aging studies in the turquoise killifish should be relevant for vertebrate aging, including humans. The rapid timescale of aging in this species should not only facilitate the causative identification of factors regulating vertebrate lifespan but also allow longitudinal studies.

The turquoise killifish has additional advantages as a model system. Contrary to many other fish, including zebrafish, the turquoise killifish has an XY-based sexual determination (Valenzano et al., 2009). Furthermore, there exists a highly inbred strain of the turquoise killifish (the GRZ strain, used in this study), as well as a number of wild-derived strains (Terzibasi et al., 2008). The availability of multiple strains provides an important advantage for genetic studies and for mapping traits that are different between strains (e.g., color, maximal lifespan) (Kirschner et al., 2012; Valenzano et al., 2009). Collectively, these characteristics of the turquoise killifish—coupled with the ease of rapidly generating many offspring and low maintenance costs—make this fish a promising vertebrate model, uniquely fit to address aging and age-related diseases (Genade et al., 2005; Valenzano et al., 2006).

For the African turquoise killifish to become a widely used vertebrate model compatible with high-throughput approaches, key tools need to be created. Although preliminary genetic tools have been developed in the turquoise killifish, including genetic linkage maps (Kirschner et al., 2012; Reichwald et al., 2009; Valenzano et al., 2009), and Tol2-based transgenesis (Hartmann and Englert, 2012; Valenzano et al., 2011), the lack of a sequenced genome and ability to manipulate endogenous genes has drastically limited the use of this organism. The RNA-guided CRISPR (clustered regularly interspaced short palindrome repeats) associated Cas9 nuclease (Jinek et al., 2012) has recently emerged as an effective approach for introducing targeted mutations in a variety of model organisms, such as yeast, worms, flies, zebrafish, and mice, as well as several non-model organisms (for a detailed list see Hsu et al. [2014]). However, genome-editing approaches have never been reported in the African turquoise killifish, probably because of the lack of a sequenced genome.

Here, we create the first platform for the rapid exploration of aging and aging-related diseases in vertebrates by developing new genomic and genome-editing tools in a promising vertebrate model, the naturally short-lived African turquoise killifish. As a proof of principle for the versatility of this platform, we generate a suite of mutated alleles for 13 genes encompassing the hallmarks of aging and report six stable lines to date. We characterize a loss-of-function mutation in the gene encoding the protein component of telomerase and show that telomerase-deficient turquoise killifish recapitulate characteristics of human pathologies. This platform should allow high-throughput studies on aging and longevity in vertebrates, as well as longitudinal modeling of human diseases. Our platform should also enable systematic examination of unexplored candidates identified in human genomic studies.

RESULTS

A Platform for the Study of "Hallmarks of Aging" Genes in Vertebrates

We sought to create a versatile platform to rapidly model human aging and diseases in the short-lived turquoise killifish (Figure 1A). A recent review has categorized nine "hallmarks of aging" (López-Otín et al., 2013), including telomere attrition, deregulated nutrient sensing, and stem cell exhaustion (Figure 1B). We selected 13 genes encompassing those hallmarks (e.g., the protein

subunit of telomerase [TERT], insulin-like growth factor 1 receptor [IGF1R], and S6 kinase [RPS6KB1]) with the overall goal of generating mutant alleles for each of them (Figure 1B).

Because the turquoise killifish is an emerging model, the first step was to identify genes in this organism. To this end, we generated a wide range of genomic data sets and designed a tailored genomic pipeline. We built gene models, using our recently assembled turquoise killifish genome (Figure 1C). We verified the accuracy of gene models and analyzed mRNA expression pattern using our RNA sequencing (RNA-seq) data sets from four tissues (Figure 1C). We generated an H3K4me3 chromatin immunoprecipitation sequencing (ChIP-seq) data set to define transcriptional start sites (TSSs) and further support annotations, especially for non-coding RNAs (Rinn and Chang, 2012) (Figure 1C). Additional support for protein-coding gene annotation was obtained using protein homology (Figure 1C). Finally, we designed guide RNA (gRNA) targets for CRISPR/Cas9 genome editing (Figure 1C and Table S1). The genome of the turquoise killifish and the RNA-seq and H3K4me3 ChIP-seq datasets are provided as resources (accession numbers JNBZ00000000, SRP041421, and SRP045718, respectively). The full description and analysis of the genome will be reported elsewhere (D.R.V., B.A.B., P.P.S., and A.B., unpublished data). The gene models and gRNA design are made available via the CHOPCHOP platform (https://chopchop.rc.fas.harvard.edu/) (Montague et al., 2014). Together, these data sets provide an integrative resource for the scientific community, not only to target specific genes in the turquoise killifish, but also for comparative genomics and evolutionary studies of aging and longevity.
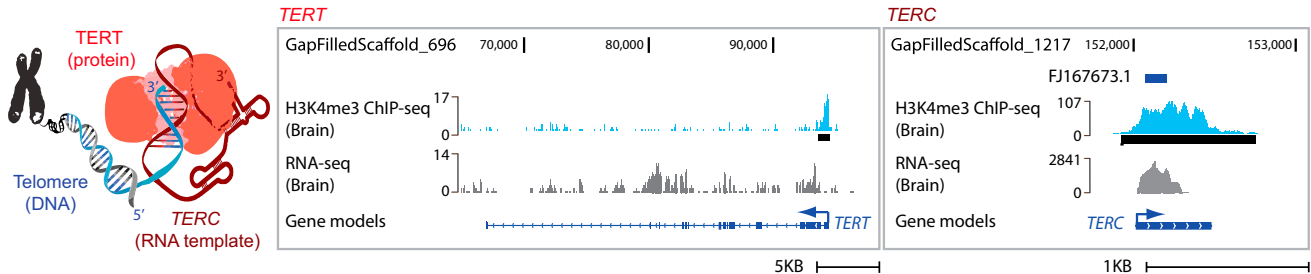
We then designed a CRISPR/Cas9 genome-editing strategy in the turquoise killifish. Based on our tailored genomic pipeline, we generated two to five independent gRNA sequences for each gene (Table S1). We then microinjected a mixture of Cas9 mRNA and gRNAs (Hwang et al., 2013; Jao et al., 2013) into fertilized turquoise killifish eggs at the single-cell stage (Figure 1D). Cas9 is known to introduce double-strand breaks that are repaired by non-homologous end joining (NHEJ), resulting in genome editing (small deletions or insertions, also known as indels) (Hsu et al., 2014). Successful editing was assessed in a subset of eggs by cloning and sequencing of the targeted region 72 hr after injection (Figure 1D, step 1). The gRNAs that resulted in successful editing were then used to generate F0 chimeras that were crossed with wild-type fish to generate F1 embryos (Figure 1D, step 2). Successful germline transmission was assessed on pooled F1 embryos, usually 45–60 days after initial injection (Figure 1D, Step 3). F1 embryos from successful F0 chimeras (founders) were raised to adulthood, and fish with desired alleles were maintained as stable lines and further backcrossed to minimize potential off-target editing by Cas9 (Figure 1D, step 4). We will first describe our results with TERT as a paradigm for modeling telomere attrition and then present the general toolbox of 13 mutant alleles in genes involved in the hallmarks of aging.
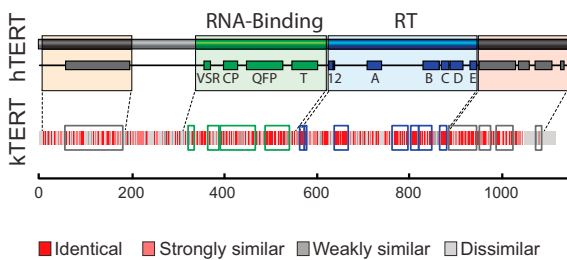
Modeling Telomere Attrition

Telomerase, which comprises the protein component TERT and the RNA component TERC, elongates telomeres after replication, thereby maintaining telomere length (Figure 2A). Telomeres
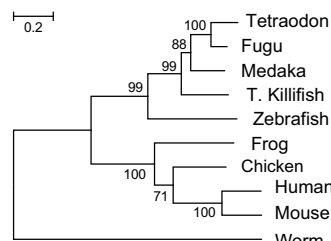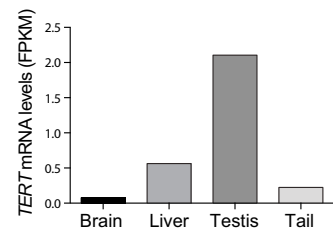
Figure 2. Example of Rapid Genome Editing of TERT, the Protein Component of Telomerase, in the Turquoise Killifish

(A) The telomerase complex and gene model prediction for *TERT* and *TERC* using genomic and epigenomic profiling.

(B) Conservation of TERT protein domains between human (hTERT) and the turquoise killifish (kTERT).

(C) TERT protein sequence divergence predicts evolutionary tree. Scale: substitution per site. Number on nodes: level of confidence.

(D) Relative expression of *TERT* mRNA in brain, liver, testis, and tail using RNA-seq. FPKM, fragments per kilobase of exon per million fragments mapped.

(E) Successful editing of the turquoise killifish *TERT* gene. The wild-type (WT) sequence, as well as the length of deletions (Δ), is indicated relative to the pro-tospacer adjacent motif (PAM, in gray) and the guide RNA sequence (gRNA, in red). The deletions that gave rise to stable lines (Δ3 and Δ8) are indicated (in yellow with black outline).

(F) Top: location of the gRNA successfully targeting *TERT* exon 2 (red line), which is upstream of the exons encoding TERT catalytic domains. *TERT* Δ8 allele is predicted to generate a protein with a premature stop codon. Bottom: the *TERT* Δ8 allele is successfully transcribed to RNA, as measured by RT-PCR followed by cDNA sequencing. RT, reverse-transcriptase.

shorten during vertebrate aging, including in the turquoise killi-fish (Artandi and DePinho, 2010; Hartmann et al., 2009), and are considered to be a good biomarker of biological age (Boone-kamp et al., 2013). In humans, mutations in *TERT* or other genes in the telomere-protecting complex result in a spectrum of dis-eases characterized by tissue homeostasis failure, such as dys-keratosis congenita (Armanios, 2009). Dyskeratosis congenita patients exhibit multiple symptoms resembling aspects of pre-mature aging, including bone marrow failure and pulmonary fibrosis (Armanios, 2009), reduced fertility (Bessler et al., 2010),

and several types of cancers (Alter et al., 2009). Because of their long telomeres, TERT-deficient laboratory mice have to be bred for four to six generations for disease phenotypes to manifest (Lee et al., 1998) and are therefore not ideal to model human TERT deficiency or telomere attrition during aging.

We first asked whether telomerase components are con-served in the turquoise killifish (Figure 2A). The *TERT* gene model (Figure 2A) allowed us to predict a putative TERT protein se-quence in the turquoise killifish. The predicted TERT protein was conserved, particularly in the RNA binding and the reverse

transcriptase (RT) catalytic domains (Figure 2B). The sequence divergence between *TERT* from the turquoise killifish and other species precisely matched the evolutionary tree (Figure 2C), confirming that the predicted TERT protein indeed corresponds to turquoise killifish TERT. Interestingly, our RNA-seq data revealed that *TERT* mRNA expression was enriched in the testis relative to other tissues in the turquoise killifish, similar to what is observed in humans (Bessler et al., 2010) (Figure 2D). *TERC*, the RNA component of telomerase, as well as other genes encoding proteins associated with telomerase (e.g., *DYSKERIN*) or involved in the protection of telomeres (e.g., *TRF2* from the Shelterin complex), were also present and expressed in the turquoise killifish (Figures 2A and S1). Thus, telomerase components are well conserved between human and the turquoise killifish.

To edit the *TERT* gene in the turquoise killifish, we designed two gRNAs with a targeting region within the *TERT* exon 2—a long exon located upstream to both catalytic domains of TERT (the RNA binding and the RT domains) (Figure 2F, top). One of the two gRNAs led to the generation of a range of deletions in the targeted region of the *TERT* gene (from 3 bp to 15 bp), with a frequency of 10% (Figure 2E). By raising the injected embryos to sexual maturity (~40 days), we obtained four F0 chimeras. Crossing each of these four chimeras with wild-type fish allowed us to generate stable lines with two different types of deletion in *TERT*: 3 bp (Δ3) and 8 bp (Δ8) (Figure 2E). The *Δ8 TERT* allele was successfully transcribed, as assessed by PCR amplification and sequencing of cDNA from heterozygous fish (Figure 2F, bottom). The *Δ8 TERT* allele is predicted to give rise to a premature stop codon in the TERT protein, N-terminal to the catalytic domains (Figure 2F). These results demonstrate the feasibility for rapid genome manipulation in the turquoise killifish, with a total time from injection to stable line of about 2 months.

A TERT-Deficient Line in the Turquoise Killifish Exhibit Loss of Telomerase Function and Are Outwardly Normal

We characterized the fish harboring the *Δ8 TERT* allele, which is predicted to result in a TERT protein without catalytic activity. To reduce the frequency of potential off-target mutations, we back-crossed *TERT$^{Δ8/+}$* fish for three generations. We then crossed these heterozygous fish with each other to generate *TERT$^{Δ8/Δ8}$* homozygous individuals (generation 1 of homozygous individuals, G1) (Figure 3A). The ratio of adult G1 *TERT$^{Δ8/Δ8}$* mutants followed the expected Mendelian ratio (p = 0.8809, χ^2 test) (Figure 3A), indicating no embryonic or juvenile (fry) lethality. Furthermore, G1 *TERT$^{Δ8/Δ8}$* embryos and adult fish were outwardly normal (Figures 3B and S2A). We asked whether the *TERT$^{Δ8/Δ8}$* allele was a true loss of function using the Telomere Repeat Amplification Protocol (TRAP) (Figure 3C). In this assay, tissue extracts are incubated with a radiolabeled oligonucleotide template, followed by PCR amplification of elongated products and autoradiography (Figure 3C). This protocol allowed us to assess telomerase enzymatic activity in liver extracts from *TERT$^{+/+}$* (wild-type) and *TERT$^{Δ8/Δ8}$* homozygous siblings (Figure 3D). Whereas liver extracts from wild-type fish showed robust telomerase activity, we failed to detect any telomerase activity in extracts from *TERT$^{Δ8/Δ8}$* fish (Figure 3D). Thus, the *Δ8* allele of *TERT*, which is predicted to generate a truncated

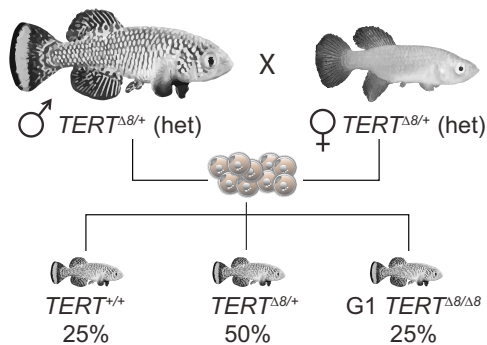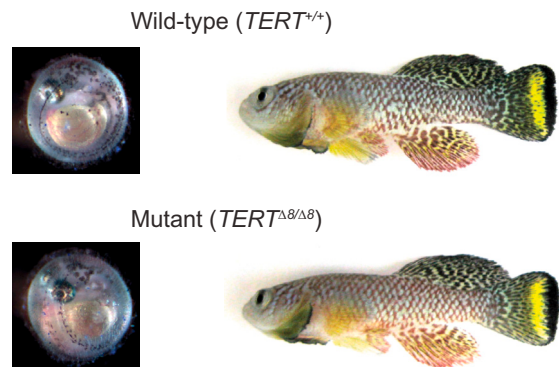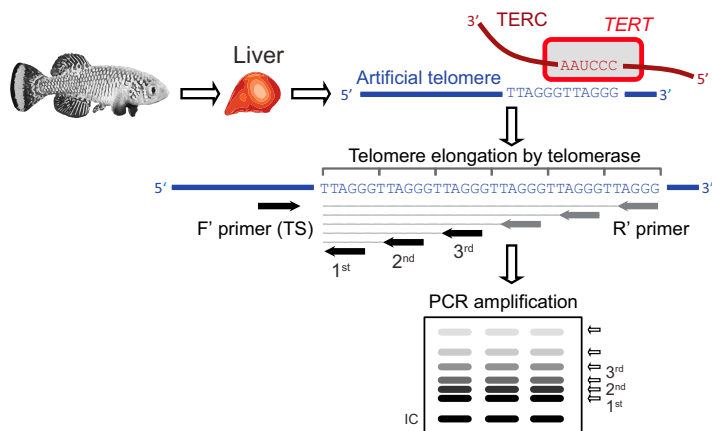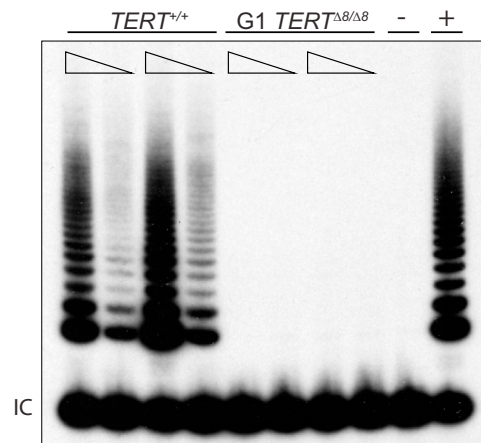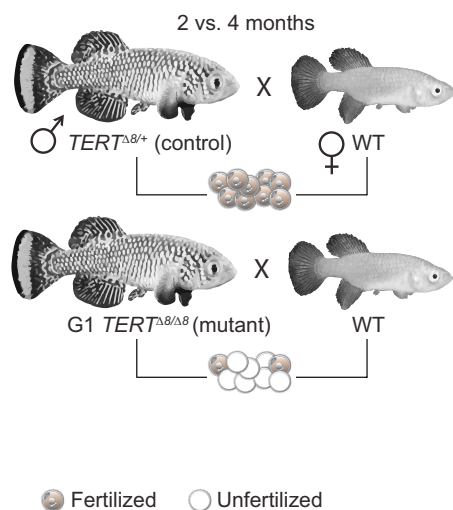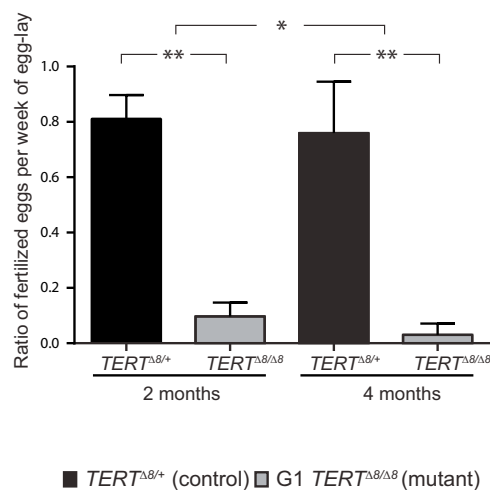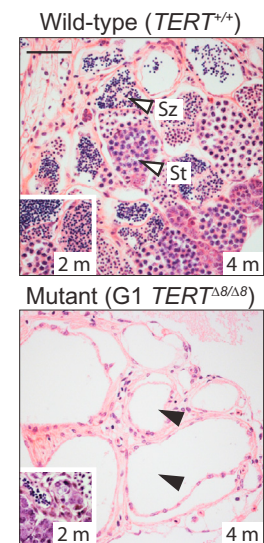TERT protein, leads to a complete loss of telomerase activity and outwardly normal individuals.

TERT-Deficient Fish Have Age-Dependent Defects in the Germline

Most human patients with haploinsufficiency for telomerase develop normally but exhibit a broad spectrum of tissue homeostasis failure (Armanios, 2009), especially in highly proliferative tissues such as blood, skin, intestine, and male germline (Bessler et al., 2010). TERT is highly expressed in the germline (Bessler et al., 2010) and is considered to be particularly important for maintaining the "immortality" of the germline (Zucchero and Ahmed, 2006). We first tested the fertility of young (2-month-old) G1 *TERT$^{Δ8/Δ8}$* males compared to control (heterozygous) siblings by crossing them to young wild-type females (Figure 3E). Whereas control heterozygous male fish were able to fertilize the majority of eggs (81%), G1 *TERT$^{Δ8/Δ8}$* males only fertilized 9% of eggs, indicating a dramatic reduction in fertility (Figure 3F, p < 0.01, Wilcoxon signed-rank test). Older G1 *TERT$^{Δ8/Δ8}$* males (4 month old) showed a further decline in fertility (Figure 3F, p < 0.05, Wilcoxon signed-rank test, comparison between age groups). Consistently, the testes of older G1 *TERT$^{Δ8/Δ8}$* males were atrophied and had an almost complete loss of germ cells compared to age-matched wild-type controls (Figure 3G, black arrowheads). Germ cells were present in younger G1 *TERT$^{Δ8/Δ8}$* males (Figure 3G, inserts), suggesting an age-dependent defect of the germline. Similarly, G1 *TERT$^{Δ8/Δ8}$* females also had atrophied ovaries (Figure S2B) and laid fewer eggs than wild-type controls (average of 7 ± 4 and 74 ± 25 eggs respectively, Figure S2B). Thus, G1 *TERT$^{Δ8/Δ8}$* fish show premature defects in their germline, resulting in infertility.

G1 *TERT$^{Δ8/Δ8}$* fish also displayed defects in other highly proliferative tissues, including blood (overall decrease in tested blood cell types, Figure S2C) and intestine (villi atrophy in some gut regions, Figure S2C). Furthermore, as previously reported in mouse models for TERT (Artandi and DePinho, 2010; Hao et al., 2005), TERT-deficient fish exhibited epithelial adenomatous changes (decreased polarity and increased nuclear/cytoplasmic ratio) (Figure S2D), which could represent a first step toward intestinal cancers such as those found in dyskeratosis congenita patients (Alter et al., 2009). In contrast, G1 *TERT$^{Δ8/Δ8}$* fish did not exhibit significant defects in low-proliferative tissues such as heart, muscle, liver, and kidney (Figure S2E). As the *TERT$^{Δ8/Δ8}$* turquoise killifish model exhibits phenotypes in the first generation (as opposed to several generations in laboratory mice [Lee et al., 1998]) and within 2 months (as opposed to 6–8 months in zebrafish [Anchelin et al., 2013; Henriques et al., 2013]), it is currently the fastest system to study telomere attrition pathologies in vertebrates.

TERT-Deficient Fish Exhibit Signs of "Genetic Anticipation"

To further explore the effect of TERT deficiency on the germline, we tested whether the offspring of TERT-deficient fish exhibit signs of "genetic anticipation." Genetic anticipation is a phenomenon in which symptoms of a genetic disorder are increased in severity or become apparent at an earlier age in the next generation, mostly due to cumulative damage in the germline.

A Design to create first generation (G1) *TERT* mutant fish

♂ *TERT*$^{\Delta 8/+}$ (het) X ♀ *TERT*$^{\Delta 8/+}$ (het)

TERT$^{+/+}$ 25%   *TERT*$^{\Delta 8/+}$ 50%   G1 *TERT*$^{\Delta 8/\Delta 8}$ 25%

B G1 *TERT*$^{\Delta 8/\Delta 8}$ fish are outwardly normal

Wild-type (*TERT*$^{+/+}$)

Mutant (*TERT*$^{\Delta 8/\Delta 8}$)

C TRAP assay

Liver

3' TERC   *TERT*

Artificial telomere 5' — TTAGGGTTAGGG — 3' AAUCCC 5'

Telomere elongation by telomerase

5' — TTAGGGTTAGGGTTAGGGTTAGGGTTAGGGTTAGGG — 3'

F' primer (TS)   R' primer

1st 2nd 3rd

PCR amplification

3rd
2nd
1st
IC

D Telomerase activity

TERT$^{+/+}$ G1 *TERT*$^{\Delta 8/\Delta 8}$ -   +

IC

E Design to test male fertility

2 vs. 4 months

♂ *TERT*$^{\Delta 8/+}$ (control) X ♀ WT

G1 *TERT*$^{\Delta 8/\Delta 8}$ (mutant) X WT

● Fertilized   ○ Unfertilized

F Male fertility

Ratio of fertilized eggs per week of egg-lay

**   *   **

TERT$^{\Delta 8/+}$ *TERT*$^{\Delta 8/\Delta 8}$ | *TERT*$^{\Delta 8/+}$ *TERT*$^{\Delta 8/\Delta 8}$

2 months   4 months

■ *TERT*$^{\Delta 8/+}$ (control) ■ G1 *TERT*$^{\Delta 8/\Delta 8}$ (mutant)

G Testis histology

Wild-type (*TERT*$^{+/+}$)

Sz
St
2 m   4 m

Mutant (G1 *TERT*$^{\Delta 8/\Delta 8}$)

2 m   4 m

(legend on next page)

Dyskeratosis congenita patients show genetic anticipation: offspring of affected individuals often exhibit earlier onset and more severe symptoms, as well as shorter telomeres (Savage and Alter, 2009). To test whether $TERT^{\Delta 8/\Delta 8}$ fish also showed signs of genetic anticipation, we crossed the G1 $TERT^{\Delta 8/\Delta 8}$ homozygous fish to generate G2 $TERT^{\Delta 8/\Delta 8}$ embryos (Figure 4A). Whereas G1 $TERT^{\Delta 8/\Delta 8}$ embryos were similar to wild-type embryos (see Figure 3B), G2 $TERT^{\Delta 8/\Delta 8}$ embryos showed gross developmental abnormalities (Figure 4B, right) and all died prior to hatching (Figure 4C). Thus, the severity of phenotype between generations increases. To test whether telomere length is indeed shorter in G2 $TERT^{\Delta 8/\Delta 8}$ embryos compared to wild-type or G1 $TERT^{\Delta 8/\Delta 8}$ embryos, we used Terminal Restriction Fragment (TRF) Southern blot on genomic DNA isolated from $TERT^{+/+}$, G1 $TERT^{\Delta 8/\Delta 8}$, or G2 $TERT^{\Delta 8/\Delta 8}$ individual live embryos using a radio-labeled telomeric probe. These Southern blots revealed that the average length of telomeres was shorter in G2 $TERT^{\Delta 8/\Delta 8}$ embryos than in wild-type embryos (~1.5 kb versus ~6 kb, respectively) (Figure 4D, left) and G1 $TERT^{\Delta 8/\Delta 8}$ embryos (Figures 4D, right, and S3). The dramatic telomere shortening in the G2 generation of TERT-deficient fish, coupled with the increase in severity of phenotype, is consistent with genetic anticipation and germline defects. Thus, we have successfully generated a vertebrate model for telomerase deficiency that rapidly recapitulates several characteristics of the corresponding human disease. Our results also provide a proof of principle for the use of genome editing in a naturally short-lived vertebrate as a powerful way to quickly test the function of a gene involved in human disease and aging.

Site-Specific Precise Editing: Generating a Disease-Causing Nucleotide Mutation in *TERT* and Inserting a Short Sequence in *POLG*

A large proportion of human diseases are not caused by deletions but by single nucleotide mutations that result in amino acid changes (non-synonymous mutations) (Abecasis et al., 2012). Therefore, we tested the feasibility of editing a specific amino acid residue, taking advantage of homology-directed repair (HDR) instead of the less precise NHEJ (Figure 5A). To this end, we co-injected Cas9 mRNA, one gRNA, and a single-strand DNA (ssDNA) template with a mutation at the desired site to modify the corresponding genomic residue via HDR (Figure 5A) (Bedell et al., 2012). In human TERT, almost all of the disease-associated mutations are non-synonymous (Podlevsky et al., 2008), and many are conserved in the turquoise killifish (Figure 5B). We selected an evolutionary conserved lysine (K902 in human TERT) whose mutation to arginine (Parry et al., 2011) or asparagine (Armanios et al., 2005) gives rise to dyskeratosis congenita. This lysine residue corresponds to K836 in the turquoise killifish (Figure 5B). To specifically edit K836, we designed a single gRNA in the proximity of the region encoding this amino acid and an ssDNA template containing two point mutations: one that changes K836 to R and another that prevents Cas9 from further targeting the edited site (Hsu et al., 2014) (Figure 5C, top). Direct sequencing indeed revealed nucleotide changes leading to the K836R mutation in the turquoise killifish TERT (Figure 5C, bottom).

We next tested the feasibility of precisely knocking in a short exogenous sequence using HDR (Figure 5A), this time targeting another candidate gene, the mitochondrial DNA Polymerase γ (*POLG*). We designed a gRNA targeting exon 2 of *POLG* and an ssDNA template containing short homology arms and an exogenous NdeI restriction sequence (Figure 5D, top). We chose to target exon 2 of *POLG*, as it has a very high targeting efficiency (90%, Figure S4). Direct sequencing or digestion with NdeI revealed in-frame knockin of the NdeI restriction site into the genomic sequence of turquoise killifish *POLG* (Figure 5D, bottom). Thus, precise genome editing allowed us to generate a specific human disease-causing mutation in the turquoise killifish *TERT* gene and knockin an exogenous sequence in the *POLG* gene.

A Toolbox of Turquoise Killifish Mutants Encompassing the Hallmark of Aging

We next sought to use our platform to target various candidate genes within the hallmarks of aging pathways (López-Otín et al., 2013), including cellular senescence and stem cell exhaustion (*p15INK4B*), mitochondrial dysfunction (*POLG*), deregulated nutrient sensing (*IGF1R*, *RAPTOR*, *RPS6KB1*, and *FOXO3*), epigenetic alterations (*ASH2L*), genomic instability (*SIRT6*), loss of proteostasis (*ATG5*), and intercellular communication (*IL8* and *APOE*) (Figures 6A and S4 and Table S1). We targeted genes whose deficiency is expected to either promote longevity (*IGF1R*, *RAPTOR*, and *RPS6KB1*) or accelerate signs of aging (*TERT* and *POLG*) (López-Otín et al., 2013). Although some

---

Figure 3. $TERT^{\Delta 8/\Delta 8}$ Fish Show No Telomerase Activity and Exhibit a Progressive Loss of Fertility in the First Generation

(A) Intercrossing of $TERT^{\Delta 8/+}$ heterozygous (het) fish to generate generation 1 (G1) $TERT^{\Delta 8/\Delta 8}$ fish. G1 $TERT^{\Delta 8/\Delta 8}$ fish are observed at the expected Mendelian ratios (no difference between expected and observed frequencies, p = 0.8809, χ^2 test).

(B) G1 $TERT^{\Delta 8/\Delta 8}$ embryos (left) and adults (right) are outwardly normal.

(C) Schematic for TRAP. Telomerase enzymatic activity in liver is evaluated by the ability of tissue extract to add telomeric repeats to radio-labeled artificial telomeres in vitro.

(D) Telomerase enzymatic activity as measured by the TRAP assay in $TERT^{+/+}$ and G1 $TERT^{\Delta 8/\Delta 8}$ fish liver samples. IC: TRAP internal control product. Representative of three independent experiments.

(E) Experimental design to assess male fertility. $TERT^{\Delta 8/+}$ (control) and G1 $TERT^{\Delta 8/\Delta 8}$ (mutant) males, at two different age groups (2 and 4 months), were mated with young (2 months) wild-type (WT) females. Fertilized eggs (gray) were counted after 1 week.

(F) Ratio of fertilized eggs per week of egg lay in $TERT^{\Delta 8/+}$ (control) and G1 $TERT^{\Delta 8/\Delta 8}$ (mutant). Mean + SD of >70 eggs, generated from 4 to 5 crosses per age group. Wilcoxon signed-rank test, *p < 0.05 and **p < 0.01. For the comparison between age groups, standardized values to age-matched controls were used.

(G) Histological sections of testis from $TERT^{+/+}$ (control) and G1 $TERT^{\Delta 8/\Delta 8}$ fish at 4 to 5 months (4 m, full-size image) and 2 months (2 m, insert). Sz, spermatozoa (mature sperm); St, spermatids. Scale bar, 50 μm. Representative of n ≥ 6 individuals from each genotype (4 to 5 months) and n = 2 individuals from each genotype (2 months). Presence of germ cells in the testis of control fish (top, white arrowheads). Deficiency of germ cells in the testis of TERT-deficient fish (bottom, black arrowheads).
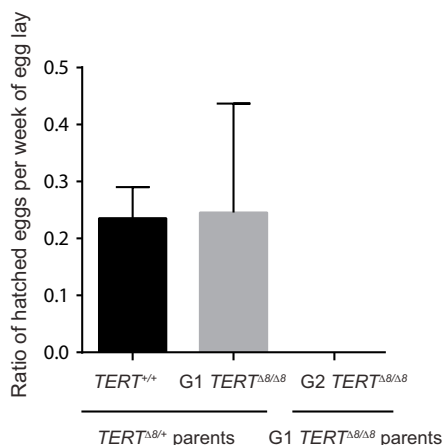
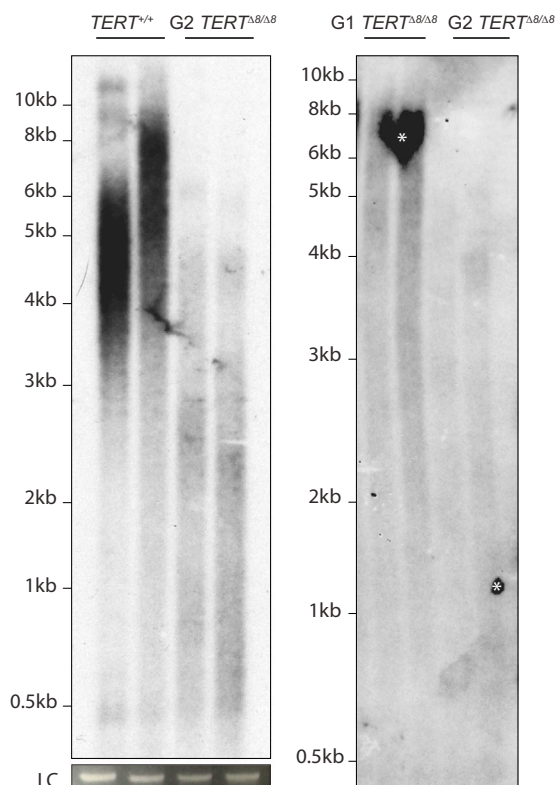**A** Design to create second generation (G2) *TERT* mutant fish

B G2 *TERT*$^{\Delta8/\Delta8}$ embryos suffer from gross abnormalities

D Telomere length measurement
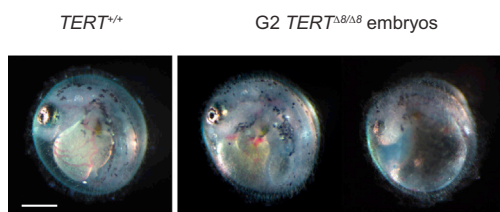
C Ratio of successful hatching per genotype

Figure 4. TERT-Deficient Turquoise Killifish Exhibit Genetic Anticipation

(A) Experimental design. G1 *TERT*$^{\Delta8/\Delta8}$ (left) or *TERT*$^{+/+}$ (right) fish were intercrossed to generate generation 2 (G2) *TERT*$^{\Delta8/\Delta8}$ or *TERT*$^{+/+}$ fish, respectively. The development of embryos was assessed until hatching.

(B) Representative images of *TERT*$^{+/+}$ and G2 *TERT*$^{\Delta8/\Delta8}$ embryos at an equivalent developmental stage. Scale bar, 300 μm.
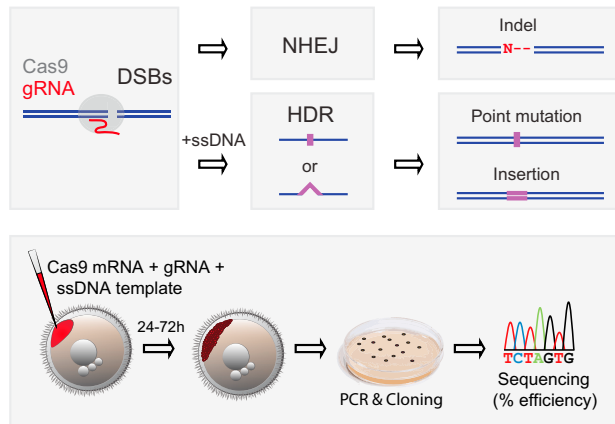
(C) Ratio of successful hatching per week of egg lay for the indicated genotypes. Mean + SD of >70 embryos for each parental genotype (*TERT*$^{\Delta8/+}$ versus G1 *TERT*$^{\Delta8/\Delta8}$).

(D) Telomere length measurement using TRF Southern blot. Left: *TERT*$^{+/+}$ and G2 *TERT*$^{\Delta8/\Delta8}$ embryos. Representative of three experiments. LC: loading control for genomic DNA. Right: G1 *TERT*$^{\Delta8/\Delta8}$ and G2 *TERT*$^{\Delta8/\Delta8}$ embryos. Expanded version is in Figure S3. White asterisk: non-specific probe binding.

genes have already been shown to regulate lifespan in both invertebrates and vertebrates (*IGF1R* and *RPS6KB1*) (Kenyon, 2010), others have not yet been tested in vertebrates (*ASH2L* and *FOXO3*) (Figure 6B). Importantly, some genes do not have obvious orthologs in yeast or invertebrates (*p15INK4B*, *IL8*, and *APOE*) (Figure 6B). Finally, several genes have been implicated in human diseases, including *APOE* (Alzheimer's disease [Rhinn et al., 2013]), *TERT* (dyskeratosis congenita [Armanios, 2009]), and *p15INK4B* (cancer [Okamoto et al., 1995]).

For each of these 13 genes, we assembled gene models and predicted protein sequences, analyzed mRNA expression patterns in four tissues, and profiled the H3K4me3 epigenetic landscape to determine TSSs (Figures 6C and S4). We designed two to five gRNA sequences for each gene (Table S1), which was sufficient to identify at least one successful gRNA (Figures 6B, 6C, and S4 and Table S1). The efficiency of targeting ranged from 0% to 90% depending on the gRNA (Figures 6 and S4 and Table S1). So far, we have

Figure 5. Precise Generation of Human Disease Mutation in *TERT* and Insertion of a Short Sequence in *POLG*

(A) Genome-editing pipeline for specific point mutations and insertions. ssDNA: ssDNA template. NHEJ: non-homologous end joining. HDR: homology-directed repair.

(B) Top: disease-associated variants in hTERT. Conservation of the disease-causing residues between human TERT and turquoise killifish TERT is color coded (red, identical; pink, similar in turquoise killifish TERT). Bottom: K902 in human TERT is evolutionary conserved and corresponds to K836 in turquoise killifish TERT.

(C) Top: location of a selected gRNA (red line) in close proximity to K836 in exon 11 of the turquoise killifish *TERT* and core sequence of the co-injected ssDNA template. Bottom: precise editing of specific codons leading to the nucleotide change (A to G) corresponding to the K836R mutation. An example chromatogram is shown at the bottom. The K836R mutation is highlighted with green background. fs, frame shift; del, deletion.
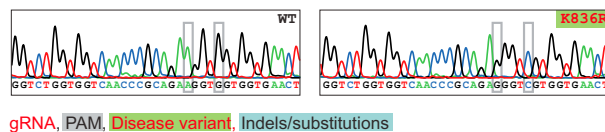
(D) Location of the gRNA targeting exon 2 of the turquoise killifish *POLG*, and core sequence of the co-injected ssDNA template to introduce an exogenous NdeI site. Bottom: precise insertion of the NdeI restriction sequence, as shown by direct sequencing or restriction digestion. Representative of two independent experiments.

generated chimeras (F0, adult) for 11 genes (Figure 6B). We have examined germline transmission for five of them (*IGF1RA*, *IGF1RB*, *ATG5*, *ASH2L*, and *RPS6KB1*) and report

the targeted alleles (Figures 6C and S4). We also have stable lines for a subset of these alleles (Figures 6B and S4 and Table S1).

A Targeted genes and pathways with stable lines

APOE CXCL8 (IL8) — Altered intercellular communication
SIRT6 — Genomic instability
Stem cell exhaustion
Telomere attrition — TERT
p15INK4B
Cellular senescence
Epigenetic alterations — ASH2L
POLG — Mitochondrial dysfunction
Loss of proteostasis — ATG5
Deregulated nutrient sensing
IGF1R FOXO3 RPS6KB1 RAPTOR
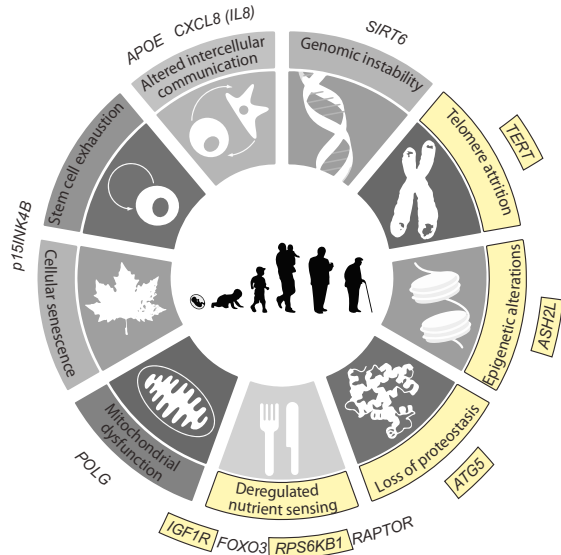
B Targeted genes and evolutionary conservation

Toolkit — Gene conservation

	Eggs	Chimera	Stable line	Human	Mouse	T. killifish	Fly	Worm	Yeast
IGF1RA									
IGF1RB									
RAPTOR									
RPS6KB1									
FOXO3									
ATG5									
SIRT6									
TERT									
POLG									
ASH2L									
CXCL8 (IL8)									
APOE									
p15INK4B									

C Selected examples of targeted genes

IGF1RA

GapFilledScaffold_349 — 160,000 — 200,000
Brain H3K4me3 ChIP-seq — 107 / 0
Brain RNA-seq — 71 / 0
Gene models — IGF1Ra
40kb

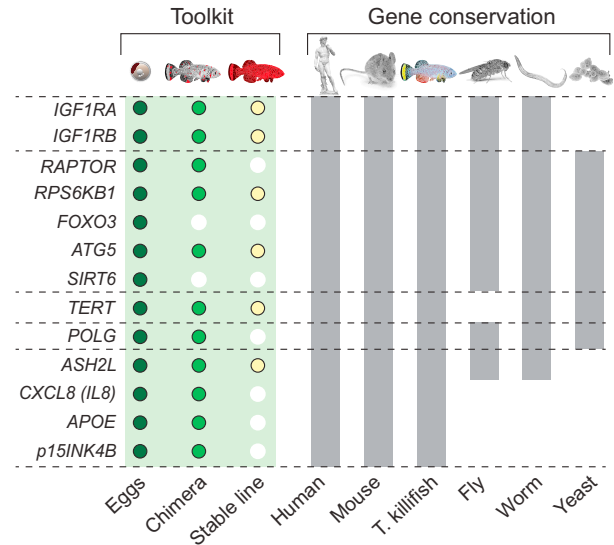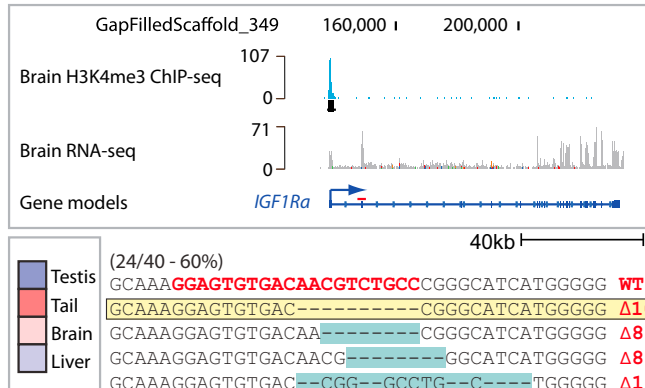|	(24/40 - 60%)	
Testis	GCAAA**GGAGTGTGACAACGTCTGCC**CGGGCATCATGGGGG	WT
Tail	GCAAAGGAGTGTGAC----------CGGGCATCATGGGGG	Δ10
Brain	GCAAAGGAGTGTGACAA--------CGGGCATCATGGGGG	Δ8
Liver	GCAAAGGAGTGTGACAACG-------GGCATCATGGGGG	Δ8
	GCAAAGGAGTGTGAC--CGG--GCCTG--C----TGGGGG	Δ1

ASH2L

GapFilledScaffold_319 — 184,000 — 190,000
Brain H3K4me3 ChIP-seq — 107 / 0
Brain RNA-seq — 148 / 0
Gene models — ASH2L
10kb

	(5/10 - 50%)	
Testis	CTGAA**GGAAATGTGCCTCACAGCTC**TGGCAAACCTCACAT	WT
Tail	CTGAAGGAAATGTGC-TGAT-GCTCTGGCAAACCTCACAT	Δ2
Brain	CTGAAGGAAATGTGC-------CTCTGGCAAACCTCACAT	Δ7
Liver	CTGAAGGAAATGTGCCTCACA----GGCAAACCTCACAT	Δ5
	CTGAAGGAAATGTGC---G---CTCTGGCAAACCTCACAT	Δ6

APOE

GapFilledScaffold_3562 — 46,000 — 48,000
Brain H3K4me3 ChIP-seq — 10 / 0
Brain RNA-seq — 3912 / 0
Gene models — APOE
2kb

Testis	AGCAG**GGAAACTTACTCTAGCTCCC**GGGTGAGCTGAGAGG	WT
Tail	AGCAGGGAAACTTACTCT-----------AGCTGAGAGG	Δ12
Brain	AGCAGGGAAACTTACTCTAGCT---GGGTGAGCTGAGAGG	Δ3
Liver	AGCAGGGAAACTTACTCTAGC--CC----GAGCTGAGAGG	Δ6
	AGCAGGGAAACTTACTCTAGC**GAGTAAGTTTCTCTAGAA**	+20

p15INK4B

GapFilledScaffold_999 — 57,000 — 59,000
Brain H3K4me3 ChIP-seq — 107 / 0
Brain RNA-seq — 83 / 0
Gene models — p15INK4B
2kb

Testis	CTGGT**GGCCGCTCAGGCTGACCCGC**AGGCCCGGGACAATC	WT
Tail	CTGGTGGCCGCTCAGGCTGACCTGCAGGCCCGGGACAATC	C/T
Brain		
Liver		

CTGGTGGCCGCTCAGGCTGACCTGCAGGCCCGGGACAATC

gRNA, Indels/substitutions, Germline transmitted (pooled F1 embryos), Stable lines, Normalized RNA expression
-1 0 -1

(legend on next page)

The platform and toolbox we have developed—genome, genomic data sets, gene models, and efficient gRNAs—as well as the mutant fish lines, will be made available to the community. To facilitate future design of gRNAs in the turquoise killifish, we have uploaded the sequenced genome and gene models into CHOPCHOP (Montague et al., 2014), thereby providing easy access for the community. Together, our results highlight the ease and versatility of our platform for generating mutants in the turquoise killifish, which will greatly facilitate high-throughput aging studies and disease modeling in vertebrates.

DISCUSSION

The Turquoise Killifish: A New Vertebrate Model for Systematic Studies on Aging and Longevity

Here, we developed a platform in a naturally short-lived vertebrate, the turquoise killifish, for the systematic exploration of aging and age-related diseases. The field of aging will greatly benefit from the study of species beyond conventional model systems (Bolker, 2012). Many exceptionally long-lived vertebrates, such as the naked mole rat (~30 years), the Brandt's bat (~30 years), capuchin monkey (~50 years), rock fish (~150 years), and the bow-headed whale (~200 years) (Tacutu et al., 2013) have already allowed comparative genomics, proteomics, and cellular studies (Austad, 2010; Gorbunova et al., 2014). However, long-lived species are not well suited for genetic manipulation, longitudinal, or lifespan studies. The turquoise killifish, with its naturally short lifespan, well-characterized aging traits, low costs, and ease of maintenance in the laboratory, is highly suited for rapid experimental aging research in vertebrates. Furthermore, the turquoise killifish is currently the shortest living vertebrate with a sequenced genome, which will be valuable for comparative studies.

Fish provide several advantages as laboratory species. They are amenable to high-throughput approaches such as genetic and drug screens (Schartl, 2014). Fish also display a range of unique traits. For example, zebrafish, the primary fish model, is widely used for developmental processes due to its unique characteristics (e.g., fast and stereotypic embryonic development). Other fish have been used for specific traits, including social behaviors (cichlids [Fernald, 2012]) and adaptive evolution (sticklebacks [Jones et al., 2012]). Our genome and genome-editing platform in the turquoise killifish should help transition this fish to a more widely studied model, providing a unique opportunity for high-throughput aging and longitudinal studies. It will be important to characterize aging in the mutants we have already generated, as well as generating additional ones. Finally, the genome-to-phenotype platform we present here could serve as a paradigm for how to rapidly develop a wide range of species into model organisms.

A Proof-of-Concept Model for Telomerase-Related Pathologies in the Turquoise Killifish

By targeting the *TERT* gene in the turquoise killifish, we have developed the fastest system so far for studying telomerase pathologies in vertebrates. Similar to what is observed in dyskeratosis congenita patients, TERT-deficient fish exhibit defects in highly proliferative tissues (male germline, intestine, and blood) in the first generation and as early as 2 months of age. This killifish *TERT* model should help untangle the interaction between aging and telomerase pathologies, which is largely unknown despite the fact that telomere attrition rate is a good predictor of accelerated aging in humans (Boonekamp et al., 2013). Although TERT-deficient killifish exhibit specific age-dependent defects, we have not observed premature death by 4–5 months of age. This might indicate that the defects in regeneration of specific tissues are not limiting for lifespan under these conditions, although they may be detrimental under more stressful conditions (e.g., injuries or end of life). It will be important to characterize lifespan, regeneration, and telomere length in this *TERT* model during aging. It will also be interesting to compare the phenotypes of this *TERT* deletion model with models mimicking in killifish the *TERT* mutations found in human patients.

The killifish model fills a unique niche in the wide range of existing models of telomerase deficiency. Cellular models have been extremely helpful to understand telomerase biology and pathologies (Batista and Artandi, 2013), but they cannot easily recapitulate systemic defects or tissue interactions. Invertebrate models, which have provided crucial insights into telomerase function (Raices et al., 2005), lack some of the organs affected by telomere pathologies in humans (e.g., bona fide blood) (Gomes et al., 2010). The main vertebrate model system, the laboratory mouse, has been the most widely used to understand the role of telomerase in specific pathologies, particularly cancer (Artandi and DePinho, 2010). However, in laboratory mouse strains, phenotypes are only manifested after several generations because of their extremely long telomeres. This issue can be solved by using the *castaneus* strain, which has shorter telomeres (Hao et al., 2005), but changing genetic background is time consuming. Recent studies in zebrafish have been promising, with TERT-deficient zebrafish demonstrating a range of phenotypes, including gastrointestinal atrophy, premature infertility, and death (Anchelin et al., 2013; Henriques et al., 2013), although it took those fish at least 6–8 months to exhibit most phenotypes. While the turquoise killifish *TERT* model is still limited by the number of available tools, it should

Figure 6. A Toolkit for Vertebrate Aging and Age-Related Disease Research
(A) Genes that were successfully edited in the nine hallmarks of aging. Genes and pathways for which we chose to generate stable lines are indicated in yellow with a black outline.
(B) Detailed stages of editing completion in specific genes, color-coded as indicated. Presence of orthologs in different species is indicated in gray.
(C) Selected examples of targeted genes depicting detailed genomic, epigenomic, and expression information (upper box), relative expression in tissues (lower left box), and types of observed indels and substitutions (lower right box). Germline-transmitted alleles assessed in pooled F1 embryos are in yellow. Stable lines are in yellow with a black outline. Whenever assessed, the targeting efficiency in eggs was indicated as a percentage. For *ASH2L*, the Δ6 stable line was generated by a separate pair of founders and was not part of the efficiency calculation. Example of a sequencing chromatogram showing the substitution in *p15INK4B*.

be well suited for rapid exploration of telomere pathologies and screening for potential treatments that can delay these pathologies.

A Toolkit for Modeling Complex Human Diseases, Traits, and Drug Responses

The advent of personalized medicine and high-throughput human genetic studies is providing an overwhelming influx of new variants associated with specific human diseases, traits, and responses to drugs (pharmacogenetics). However, functional validation for most of these genes and variants is lagging behind. One way to study these candidates has been to generate induced pluripotent stem cells (iPSCs) harboring mutations derived from patients or engineered de novo (Hockemeyer et al., 2011). Although this approach allows high-throughput studies, it does not recapitulate the complex interactions between tissues, such as endocrine and paracrine communication, as well as complex responses to environment or drugs. The turquoise killifish model could greatly facilitate in vivo high-throughput studies of new candidate genes or alleles, while modeling the integrative and non-cell-autonomous interactions that are characteristic of aging and pathological conditions.

Recent genomic studies have revealed that many human diseases are caused by deleterious non-synonymous variants (Abecasis et al., 2012), and this is also likely the case for aging and longevity. For example, most disease-causing mutations in human *TERT* are due to variants leading to a single amino acid residue change (Podlevsky et al., 2008). Here, we show the feasibility of editing specific sequences in turquoise killifish genes. Such directed knockin approach will also be particularly helpful for the systematic exploration of variants in human longevity candidate genes, such as *IGF1R*, which is among ~200 predicted candidates identified by genetic association studies of longevity (Tacutu et al., 2013). This approach could also facilitate introduction of epitope tags, *loxP* sites, or artificial stop codons at endogenous genomic loci.

Overall, our study provides a rapid pipeline for genotype-to-phenotype analyses in a new vertebrate model with a compressed timescale of aging. It also renders available as a resource the de novo sequenced genome of the turquoise killifish and mutant lines of this fish. This comprehensive platform opens the possibility of screening for genetic and drug interactions in an integrative system. In addition, it offers a promising venue for high-throughput modeling of aging and complex human diseases in vivo.

EXPERIMENTAL PROCEDURES

Additional details are provided in the Extended Experimental Procedures.

Gene Model Prediction, Conservation, and Phylogeny

Gene models were obtained from two independent sources: (1) a de novo whole-genome shotgun assembly (GenBank JNBZ00000000) and (2) a de novo transcriptome assembly from four adult fish tissues (brain, liver, testis, and tail) using Oases (Schulz et al., 2012) (Sequence Read Archive [SRA] SRP041421). For the de novo transcriptome assembly, putative annotations were obtained by unidirectional blastx to the Swissprot database. The detailed genome assembly and annotation will be reported elsewhere (D.R.V., B.A.B., P.P.S., and A.B., unpublished data).

Strand-Specific RNA-Seq Expression Analysis

RNA extraction was performed using the Nucleospin kit (Machery-Nagel), followed by rRNA removal (Ribozero Magnetic Gold Kit, Epicenter). Double-strand cDNA was ligated with barcoded adapters and amplified using Illumina PCR primers (P1.0 and 2.0, Illumina) prior to sequencing. Expression data were analyzed by mapping RNA-seq reads onto gene models using Tophat2 v2.0.4 and Cufflinks v2.0.2.

H3K4me3 ChIP-Seq

H3K4me3 ChIP-seq experiments were performed according to Benayoun et al. (2014) on whole-brain tissue isolated from adult male fish (SRA SRP045718).

CRISPR/Cas9 Target Prediction for Guide RNA Selection

For each selected gene, we identified conserved regions in the coding sequence using multiple vertebrate orthologs using http://genome.ucsc.edu/. Conserved regions that were upstream of functional or active protein domains were selected for targeting. gRNA target sites were identified using ZiFiT (http://zifit.partners.org/) (Hwang et al., 2013) or CHOPCHOP (https://chopchop.rc.fas.harvard.edu/) (Montague et al., 2014).

Guide RNA Synthesis

Initial experiments were performed using the DR274 guide RNA expression vector (Addgene, 42250) (Hwang et al., 2013). In subsequent experiments, hybridized oligonucleotides were used as an in vitro transcription template. gRNAs were in vitro transcribed and purified using the MAXIscript T7 kit (Life Technologies).

Production of Cas9 mRNA

Initial experiments were performed using the MLM3613 Cas9 expression vector (Addgene, 42251) (Hwang et al., 2013). In subsequent experiments, the pCS2-nCas9n expression vector was used (Addgene, 47929) (Jao et al., 2013). Capped and polyadenylated Cas9 mRNA was in vitro transcribed and purified using either the mMESSAGE mMACHINE T7 ULTRA or SP6 kits (Life Technologies).

Single-Stranded DNA Template for Homology-Directed Repair

For homology-directed repair (HDR) experiments, ssDNA templates were designed to contain short homology arms (30 bp–50 bp) surrounding the gRNA target. The ssDNA templates were commercially synthesized and purified prior to injection (QIAquick Nucleotide Removal Kit, QIAGEN) (Bedell et al., 2012).

Microinjection of Turquoise Killifish Embryos and Sequencing of Targeted Sites

Microinjection of turquoise killifish embryos was performed according to Valenzano et al. (2011). Cas9-encoding mRNA (200–300 ng/μl) and gRNA (30 ng/μl) were mixed with phenol-red (2%) and co-injected into one-cell-stage fish embryos. For HDR experiments, the ssDNA template (20 μM) was also co-injected. Three days after injection, genomic DNA was extracted from five to ten pooled embryos. The genomic area encompassing the targeted site (~600 bp) was PCR amplified. Endonuclease digestions or DNA sequencing was used for analysis (Table S1).

Fish husbandry, telomerase activity and telomere length measurements, fertility, histology, and blood count analyses are provided in the Extended Experimental Procedures.

ACCESSION NUMBERS

Sequencing and genome data have been deposited to the GenBank (JNBZ00000000). RNA-seq (SRP041421) and H3K4me3 ChIP-seq (SRP045718) data were submitted to SRA (Sequence Read Archive).

SUPPLEMENTAL INFORMATION

Supplemental Information includes Extended Experimental Procedures, four figures, and one table and can be found with this article online at http://dx.doi.org/10.1016/j.cell.2015.01.038.

AUTHOR CONTRIBUTIONS

ACKNOWLEDGMENTS

REFERENCES

Abecasis, G.R., Auton, A., Brooks, L.D., DePristo, M.A., Durbin, R.M., Handsaker, R.E., Kang, H.M., Marth, G.T., and McVean, G.A.; 1000 Genomes Project Consortium (2012). An integrated map of genetic variation from 1,092 human genomes. Nature 491, 56–65.

Alter, B.P., Giri, N., Savage, S.A., and Rosenberg, P.S. (2009). Cancer in dyskeratosis congenita. Blood 113, 6549–6557.

Anchelin, M., Alcaraz-Pérez, F., Martínez, C.M., Bernabé-García, M., Mulero, V., and Cayuela, M.L. (2013). Premature aging in telomerase-deficient zebrafish. Dis. Model. Mech. 6, 1101–1112.

Armanios, M. (2009). Syndromes of telomere shortening. Annu. Rev. Genomics Hum. Genet. 10, 45–61.

Armanios, M., Chen, J.L., Chang, Y.P., Brodsky, R.A., Hawkins, A., Griffin, C.A., Eshleman, J.R., Cohen, A.R., Chakravarti, A., Hamosh, A., and Greider, C.W. (2005). Haploinsufficiency of telomerase reverse transcriptase leads to anticipation in autosomal dominant dyskeratosis congenita. Proc. Natl. Acad. Sci. USA 102, 15960–15964.

Artandi, S.E., and DePinho, R.A. (2010). Telomeres and telomerase in cancer. Carcinogenesis 31, 9–18.

Austad, S.N. (2010). Cats, "rats," and bats: the comparative biology of aging in the 21st century. Integr. Comp. Biol. 50, 783–792.

Batista, L.F., and Artandi, S.E. (2013). Understanding telomere diseases through analysis of patient-derived iPS cells. Curr. Opin. Genet. Dev. 23, 526–533.

Bedell, V.M., Wang, Y., Campbell, J.M., Poshusta, T.L., Starker, C.G., Krug, R.G., 2nd, Tan, W., Penheiter, S.G., Ma, A.C., Leung, A.Y., et al. (2012). In vivo genome editing using a high-efficiency TALEN system. Nature 491, 114–118.

Benayoun, B.A., Pollina, E.A., Ucar, D., Mahmoudi, S., Karra, K., Wong, E.D., Devarajan, K., Daugherty, A.C., Kundaje, A.B., Mancini, E., et al. (2014). H3K4me3 breadth is linked to cell identity and transcriptional consistency. Cell 158, 673–688.

Bessler, M., Wilson, D.B., and Mason, P.J. (2010). Dyskeratosis congenita. FEBS Lett. 584, 3831–3838.

Bolker, J. (2012). Model organisms: There's more to life than rats and flies. Nature 491, 31–33.

Boonekamp, J.J., Simons, M.J., Hemerik, L., and Verhulst, S. (2013). Telomere length behaves as biomarker of somatic redundancy rather than biological age. Aging Cell 12, 330–332.

Di Cicco, E., Tozzini, E.T., Rossi, G., and Cellerino, A. (2011). The short-lived annual fish Nothobranchius furzeri shows a typical teleost aging process reinforced by high incidence of age-dependent neoplasias. Exp. Gerontol. 46, 249–256.

Fernald, R.D. (2012). Social control of the brain. Annu. Rev. Neurosci. 35, 133–151.

Genade, T., Benedetti, M., Terzibasi, E., Roncaglia, P., Valenzano, D.R., Cattaneo, A., and Cellerino, A. (2005). Annual fishes of the genus Nothobranchius as a model system for aging research. Aging Cell 4, 223–233.

Gomes, N.M., Shay, J.W., and Wright, W.E. (2010). Telomere biology in Metazoa. FEBS Lett. 584, 3741–3751.

Gorbunova, V., Seluanov, A., Zhang, Z., Gladyshev, V.N., and Vijg, J. (2014). Comparative genetics of longevity and cancer: insights from long-lived rodents. Nat. Rev. Genet. 15, 531–540.

Hao, L.Y., Armanios, M., Strong, M.A., Karim, B., Feldser, D.M., Huso, D., and Greider, C.W. (2005). Short telomeres, even in the presence of telomerase, limit tissue renewal capacity. Cell 123, 1121–1131.

Hartmann, N., and Englert, C. (2012). A microinjection protocol for the generation of transgenic killifish (Species: Nothobranchius furzeri). Dev. Dyn. 241, 1133–1141.

Hartmann, N., Reichwald, K., Lechel, A., Graf, M., Kirschner, J., Dorn, A., Terzibasi, E., Wellner, J., Platzer, M., Rudolph, K.L., et al. (2009). Telomeres shorten while Tert expression increases during ageing of the short-lived fish Nothobranchius furzeri. Mech. Ageing Dev. 130, 290–296.

Henriques, C.M., Carneiro, M.C., Tenente, I.M., Jacinto, A., and Ferreira, M.G. (2013). Telomerase is required for zebrafish lifespan. PLoS Genet. 9, e1003214.

Hockemeyer, D., Wang, H., Kiani, S., Lai, C.S., Gao, Q., Cassady, J.P., Cost, G.J., Zhang, L., Santiago, Y., Miller, J.C., et al. (2011). Genetic engineering of human pluripotent cells using TALE nucleases. Nat. Biotechnol. 29, 731–734.

Hsu, P.D., Lander, E.S., and Zhang, F. (2014). Development and applications of CRISPR-Cas9 for genome engineering. Cell 157, 1262–1278.

Hwang, W.Y., Fu, Y., Reyon, D., Maeder, M.L., Tsai, S.Q., Sander, J.D., Peterson, R.T., Yeh, J.R., and Joung, J.K. (2013). Efficient genome editing in zebrafish using a CRISPR-Cas system. Nat. Biotechnol. 31, 227–229.

Jao, L.E., Wente, S.R., and Chen, W. (2013). Efficient multiplex biallelic zebrafish genome editing using a CRISPR nuclease system. Proc. Natl. Acad. Sci. USA 110, 13904–13909.

Jinek, M., Chylinski, K., Fonfara, I., Hauer, M., Doudna, J.A., and Charpentier, E. (2012). A programmable dual-RNA-guided DNA endonuclease in adaptive bacterial immunity. Science 337, 816–821.

Jones, F.C., Grabherr, M.G., Chan, Y.F., Russell, P., Mauceli, E., Johnson, J., Swofford, R., Pirun, M., Zody, M.C., White, S., et al.; Broad Institute Genome Sequencing Platform & Whole Genome Assembly Team (2012). The genomic basis of adaptive evolution in threespine sticklebacks. Nature 484, 55–61.

Kenyon, C.J. (2010). The genetics of ageing. Nature 464, 504–512.

Kirschner, J., Weber, D., Neuschl, C., Franke, A., Böttger, M., Zielke, L., Powalsky, E., Groth, M., Shagin, D., Petzold, A., et al. (2012). Mapping of quantitative trait loci controlling lifespan in the short-lived fish Nothobranchius furzeri—a new vertebrate model for age research. Aging Cell 11, 252–261.

Lee, H.W., Blasco, M.A., Gottlieb, G.J., Horner, J.W., 2nd, Greider, C.W., and DePinho, R.A. (1998). Essential role of mouse telomerase in highly proliferative organs. Nature 392, 569–574.

López-Otín, C., Blasco, M.A., Partridge, L., Serrano, M., and Kroemer, G. (2013). The hallmarks of aging. Cell 153, 1194–1217.

Montague, T.G., Cruz, J.M., Gagnon, J.A., Church, G.M., and Valen, E. (2014). CHOPCHOP: a CRISPR/Cas9 and TALEN web tool for genome editing. Nucleic Acids Res. 42, W401–W407.

Niccoli, T., and Partridge, L. (2012). Ageing as a risk factor for disease. Curr. Biol. *22*, R741–R752.

Okamoto, A., Hussain, S.P., Hagiwara, K., Spillare, E.A., Rusin, M.R., Demetrick, D.J., Serrano, M., Hannon, G.J., Shiseki, M., Zariwala, M., et al. (1995). Mutations in the p16INK4/MTS1/CDKN2, p15INK4B/MTS2, and p18 genes in primary and metastatic lung cancer. Cancer Res. *55*, 1448–1451.

Parry, E.M., Alder, J.K., Qi, X., Chen, J.J., and Armanios, M. (2011). Syndrome complex of bone marrow failure and pulmonary fibrosis predicts germline defects in telomerase. Blood *117*, 5607–5611.

Podlevsky, J.D., Bley, C.J., Omana, R.V., Qi, X., and Chen, J.J. (2008). The telomerase database. Nucleic Acids Res. *36*, D339–D343.

Raices, M., Maruyama, H., Dillin, A., and Karlseder, J. (2005). Uncoupling of longevity and telomere length in *C. elegans*. PLoS Genet. *1*, e30.

Reichwald, K., Lauber, C., Nanda, I., Kirschner, J., Hartmann, N., Schories, S., Gausmann, U., Taudien, S., Schilhabel, M.B., Szafranski, K., et al. (2009). High tandem repeat content in the genome of the short-lived annual fish *Nothobranchius furzeri*: a new vertebrate model for aging research. Genome Biol. *10*, R16.

Rhinn, H., Fujita, R., Qiang, L., Cheng, R., Lee, J.H., and Abeliovich, A. (2013). Integrative genomics identifies APOE ε4 effectors in Alzheimer's disease. Nature *500*, 45–50.

Rinn, J.L., and Chang, H.Y. (2012). Genome regulation by long noncoding RNAs. Annu. Rev. Biochem. *81*, 145–166.

Savage, S.A., and Alter, B.P. (2009). Dyskeratosis congenita. Hematol. Oncol. Clin. North Am. *23*, 215–231.

Schartl, M. (2014). Beyond the zebrafish: diverse fish species for modeling human disease. Dis. Model. Mech. *7*, 181–192.

Schulz, M.H., Zerbino, D.R., Vingron, M., and Birney, E. (2012). Oases: robust de novo RNA-seq assembly across the dynamic range of expression levels. Bioinformatics *28*, 1086–1092.

Tacutu, R., Craig, T., Budovsky, A., Wuttke, D., Lehmann, G., Taranukha, D., Costa, J., Fraifeld, V.E., and de Magalhães, J.P. (2013). Human Ageing Genomic Resources: integrated databases and tools for the biology and genetics of ageing. Nucleic Acids Res. *41*, D1027–D1033.

Terzibasi, E., Valenzano, D.R., Benedetti, M., Roncaglia, P., Cattaneo, A., Domenici, L., and Cellerino, A. (2008). Large differences in aging phenotype between strains of the short-lived annual fish *Nothobranchius furzeri*. PLoS ONE *3*, e3866.

Terzibasi, E., Lefrançois, C., Domenici, P., Hartmann, N., Graf, M., and Cellerino, A. (2009). Effects of dietary restriction on mortality and age-related phenotypes in the short-lived fish *Nothobranchius furzeri*. Aging Cell *8*, 88–99.

Trancikova, A., Ramonet, D., and Moore, D.J. (2011). Genetic mouse models of neurodegenerative diseases. Prog. Mol. Biol. Transl. Sci. *100*, 419–482.

Valenzano, D.R., Terzibasi, E., Cattaneo, A., Domenici, L., and Cellerino, A. (2006). Temperature affects longevity and age-related locomotor and cognitive decay in the short-lived fish *Nothobranchius furzeri*. Aging Cell *5*, 275–278.

Valenzano, D.R., Kirschner, J., Kamber, R.A., Zhang, E., Weber, D., Cellerino, A., Englert, C., Platzer, M., Reichwald, K., and Brunet, A. (2009). Mapping loci associated with tail color and sex determination in the short-lived fish *Nothobranchius furzeri*. Genetics *183*, 1385–1395.

Valenzano, D.R., Sharp, S., and Brunet, A. (2011). Transposon-mediated transgenesis in the short-lived African killifish *Nothobranchius furzeri*, a vertebrate model for aging. G3 (Bethesda) *1*, 531–538.

Zucchero, T., and Ahmed, S. (2006). Genetics of proliferative aging. Exp. Gerontol. *41*, 992–1000.

Supplemental Information

EXTENDED EXPERIMENTAL PROCEDURES

Turquoise Killifish Care and Husbandry

Turquoise killifish (GRZ strain) were housed at 26°C in a central filtration recirculating system (Aquaneering, San Diego) with a 12 hr light/dark cycle (Valenzano et al., 2011). Fish were fed twice a day with freeze-dried bloodworms (Hikari, Japan). All turquoise killifish care and uses were approved by the Stanford Subcommittee on Research Animal Care.

Gene Model Prediction, Conservation, and Phylogeny

Gene models were obtained from two independent sources: i) a de novo transcriptome assembly from 4 adult fish tissues (brain, liver, testis, tail) using the de Bruijn graph assembler Oases (Schulz et al., 2012) and ii) a de novo whole genome shotgun assembly (GenBank JNBZ00000000 accession) (details will be provided elsewhere [D.R.V., B.A.B., P.P.S., and A.B., unpublished data]). For the de novo transcriptome assembly, putative annotations were obtained by unidirectional blastx to the Swissprot database. The genome was annotated using the MAKER2 pipeline (Holt and Yandell, 2011), using trained SNAP and Augustus gene predictors, and further support from turquoise killifish transcriptome (previously published transcripts [Petzold et al., 2013], our assembled transcripts and raw RNA-seq reads), transcripts from the closely related killifish *H. fondulus*, and proteins sequences from other teleosts (*D. rerio*, *O. latipes*, *T. rubripes*). Annotation of putative gene models was obtained by reciprocal best BLAT hit to species-specific Uniprot reference proteomes.

To calculate the phylogeny and conservation of TERT, boundaries of the conserved TERT domains for the human TERT sequence were obtained from Telomerase Database (Podlevsky et al., 2008) and their positions were mapped to the turquoise killifish TERT protein based on the alignment between human and killifish TERT sequences. Gonnet (Position Accepted Mutations 250) matrix in ClustalW2 (http://www.ebi.ac.uk/Tools/msa/clustalw2/) was used to categorize each killifish TERT amino acid as Identical, Strongly similar (Position Accepted Mutations > 0.5), Weakly similar (Position Accepted Mutations < 0.5) and Dissimilar (Figure 2B). The maximum likelihood phylogenetic tree of the TERT sequence from 10 species (Figure 2C) was constructed using MEGA6 (Tamura et al., 2013), with 1,000 bootstrap steps for statistical support.

Strand-Specific RNA-Seq Expression Analysis

To extract mRNA from tissues, Nucleospin kit (Machery-Nagel) was used, followed by Ribozero Magnetic Gold Kit for rRNA removal. The rRNA-depleted samples were further concentrated and purified by AMPure RNAClean XP beads, and then fragmented by incubating with RNA fragmentation buffer at 94°C for 5 min. For first-strand cDNA synthesis, random hexamer, Oligo dT primers (3μg/μl), and SuperScript III RT (Invitrogen) were used. The second-strand cDNAs were synthesized with a mixture of dNTPs and dUTPs. After end-repairing (Epicenter), double-strand cDNAs were ligated with barcoded adapters. dUTP-labeled second strand cDNAs were removed by Uracil-N-Glycosylase treatment (Applied Biosystems), and the first-strand cDNAs were amplified by Phusion DNA polymerase (NEB) and Illumina PCR primers P 1.0 and 2.0 (Illumina). Expression data were analyzed by mapping RNA-seq reads onto gene models using Tophat2 v2.0.4 and Cufflinks v2.0.2 (Trapnell et al., 2012), using upper quartile normalization to enable cross tissues comparisons (accession number SRP041421).

H3K4me3 ChIP-Seq

H3K4me3 ChIP-seq experiments on turquoise killifish brain were performed as previously described (Benayoun et al., 2014). Briefly, brain tissues from adult male fish were minced manually prior to crosslinking. Chromatin was sheared with a Vibra-Cell Sonicator VC130 (Sonics) in RIPA buffer (1% NP-40, 0.5% sodium deoxycholate in PBS pH 7.4), and immunoprecipitated with 5 μl of H3K4me3 antibody (Active Motif antibody 39159). Libraries were generated according to Illumina instructions, and PCR amplified for 18 cycles. A control input library was also generated. Reads of 36 bp were generated on an Illumina Genome Analyzer II. Reads were quality-filtered, then mapped to our turquoise killifish genome build (GenBank JNBZ00000000, assembly will be described elsewhere (D.R.V., B.A.B., P.P.S., and A.B., unpublished data) using bowtie0.12.7 (Langmead et al., 2009). ChIP-seq peaks were called using the MACS2.08 software against the input library (Feng et al., 2012).

CRISPR/Cas9 Target Prediction for Guide RNA Selection

For each gene model, the coding sequence was analyzed according to level of vertebrate conservation, as well as conservation to Medaka (evolutionary closest sequenced teleost) using http://genome.ucsc.edu/. Regions upstream to functional or active domains of the protein (usually in exons 1-3) were targeted. Guide RNA (gRNA) target sites were identified to meet the following criteria: 5′-GG-(N)18-NGG-3′ by using ZiFiT (http://zifit.partners.org/) (Hwang et al., 2013) and CHOPCHOP (Montague et al., 2014). In some cases, targets were chosen according to the presence of a unique restriction site proximal to the protospacer adjacent motif (PAM) site to facilitate identification of successful editing. ZiFiT returns a list of the sequences of oligonucleotides that can be synthesized and cloned into pDR274 vector to create gRNA expression plasmid (Hwang et al., 2013). Targets identified by ZiFiT or CHOPCHOP were also used for the oligonucleotide-based high throughput approach to synthesize the "variable oligonucleotide" (see below).

Guide RNA Synthesis

Initial experiments were performed according to Hwang et al. (2013), using the DR274 guide RNA expression vector (Addgene #42250). In subsequent experiments (for *p15INK4B/CDKN2B*, *IL8/CXCL8*, *SIRT6*, *FOXO3*, *APOE*, *ATG5*, *RAPTOR*, and *RPS6KB1*),

a high throughput approach was used ([Gagnon et al., 2014](#)), with hybridized oligonucleotides as an in vitro transcription template. For example, to target the following genomic sequence **GG**ACAACGTCAACCAGGGGG (turquoise killifish *RPS6KB1*), a universal reverse oligonucleotide (5′-AAAAGCACCGACTCGGTGCCACTTTTTCAAGTTGATAACGGACTAGCCTTATTTTAACTTGCTATTTCTAGCTC TAAAAC-3′) and a variable oligonucleotide that contains the target sequence (5′-TAATACGACTCACTATAGGACAACGTCAAC CAGGGGGGTTTTAGAGCTAGAAATAGCAAG-3′) were annealed. For the annealing procedure, 1 μl from each oligonucleotide (200μM stock) were annealed in annealing buffer (50 mM NaCl, 10 mM Tris-HCl, 10 mM MgCl2, 1 mM DTT pH 7.9) using the following program: 95°C (30 s), 72°C (2 min), 37°C (2 min), 25°C (2 min), 12°C (2 min), 4°C (2 min). After annealing, single-stranded overhangs were filled by T4 DNA polymerase reaction according to manufacturer's instructions (New England Biolabs) and the resulting product was used as a template for RNA synthesis. gRNAs were transcribed with the MAXIscript T7 kit (Life Technologies) using either the DraI-digested DR274 gRNA expression vector or annealed oligonucleotides as templates. gRNAs were purified using GlycoBlue (Life Technologies) with EtOH/ammonium acetate precipitation and resuspended in RNase-free water.

Production of Cas9 mRNA

For synthesis of Cas9 mRNA, MLM3613 expression vector was linearized by PmeI digestion, and purified using EtOH/ammonium acetate precipitation. Capped Cas9 mRNA was synthesized using the mMESSAGE mMACHINE T7 ULTRA kit (Life Technologies, as directed). Following completion of transcription, the poly(A) tailing reaction and DNaseI treatment were performed according to the manufacturer's instructions (Life Technologies). For synthesis of nuclear Cas9 (nCas9n) mRNA, pCS2-nCas9n was linearized by NotI digestion. Capped and polyadenylated nCas9n mRNA was synthesized using mMESSAGE mMACHINE SP6 (Life Technologies). Both Cas9 and nCas9n mRNAs were purified as described above for the gRNAs.

The *TERT* gene targeting experiment was performed according to [Hwang et al. (2013)](#), using MLM3613 Cas9 expression vector (Addgene, #42251). Subsequent experiments were performed using pCS2-nCas9n ([Jao et al., 2013](#)) (Addgene, #47929).

Single-Stranded DNA Template for HDR

Single-stranded DNA (ssDNA) template was designed to contain homology arms (∼30bp - 50bp) surrounding the gRNA target site. In order to generate the K836R mutation in the killifish *TERT* gene, the following ssDNA sequence was used as template (point mutations are in square brackets): CTGGAGTGCCGCAGTATGGTCTGGTGGTCAACCCGCAGA[G]GGT[C]GTGGTGAACTTTCCGATAC CAGAACGTCCATGGTCT.

For *POLG*, the ssDNA sequence was modified to knock-in an exogenous NdeI site (i.e., CATATG) if successful editing took place. This approach was selected to facilitate identification of HDR events by using NdeI digestion. Successful HDR would also modify the genomic gRNA target sequence (i.e., PAM sequence), protecting it from further CRISPR-mediated editing. The following ssDNA sequence was used as template (modified codons are in square brackets): ATCTTCCATGGGGTTGTGCCGGAGTACAGA[CAT ATG]GATGTGGAGCGCAGCATCAAGCATTTAGAGAAGCACAAGCTGTGGGGGAAG.

Microinjection of Turquoise Killifish Embryos and Sequencing of Mutated Target Sites

Microinjection of turquoise killifish embryos was done according to [Valenzano et al. (2011)](#). gRNA and Cas9-encoding mRNA were co-injected into one-cell stage turquoise killifish embryos. Each embryo was injected with a solution containing ∼30ng/μl of gRNA and ∼200-300ng/μl of Cas9 mRNA, and 2% phenol-red (for visualization). For HDR experiments, the ssDNA template at a final concentration of 20μM was also co-injected. Three days after injection, genomic DNA was extracted from 5-10 pooled embryos. The genomic area encompassing the targeted site (∼600bp) was PCR-amplified, and endonuclease digestions ([Table S1](#)) or DNA sequencing were used for further analysis. We observed that a molar ratio of 1:3 of Cas9 and the gRNA transcripts gave rise to almost complete targeting, with up to 90% of the sequences targeted in *POLG* (both alleles), suggesting optimal conditions. These concentrations are similar to what was previously reported in zebrafish ([Hwang et al., 2013](#)).

Targeted loci were amplified from turquoise killifish genomic DNA using primers designed to anneal approximately 300-400 base pairs upstream and downstream from the expected targeted site and AccuPrime Pfx DNA Polymerase (Life Technologies) or GoTaq Green Master Mix (Promega) were used. For analysis by DNA digestion, PCR products were purified using PCR purification kit (QIAGEN), and digested using the appropriate enzyme (New England Biolabs, see [Table S1](#)). Successful targeting was evaluated according to the proportion of undigested product in the injected embryos, compared to the fully digested PCR product in the non-targeted control genomic DNA. A list of the primers used in this study is provided in ([Table S1](#)). For analysis by DNA sequencing, each target site was amplified and purified as described above. The resulting PCR products were cloned into a plasmid using TOPO-TA PCR cloning kit (Life Technologies). Following transformation of the reactions, single colonies were selected, and DNA isolated from overnight cultures was sequenced by Sanger sequencing. Successful editing was identified by comparison to the wild-type sequence. In order to confirm single base substitutions, sequencing of pooled eggs was performed twice on independent batches.

TRAP and TRF Analysis

Telomere Repeat Amplification Protocol (TRAP) was carried out according to [Zhong et al. (2012)](#) using the Trapeze kit (Milipore). Isolated livers were snap-frozen in liquid nitrogen, crushed into a powder, and lysed in NP40 buffer (25 mM HEPES-KOH, 400 mM NaCl, 1.5 mM MgCl$_2$, 10% glycerol, 0.5% NP40, and 1 mM DTT [pH 7.5] supplemented with protease inhibitors). Each reaction was

programmed with 0.25–1 μg of protein lysate according to the kit instructions. Following PCR amplification (25 cycles), reactions were resolved on 30% polyacrylamide gel and visualized using autoradiography.

TRF was performed according to Zhong et al. (2012), and further adapted to low amounts of DNA. Genomic DNA was extracted from single embryos using proteinase K, purified using phenol/chloroform/isoamyl alcohol, and digested over-night with RsaI and HinfI. Digested samples were resolved using electrophoresis followed by Southern blotting with a telomeric specific end-radiolabeled (TTAGGG)$_4$ oligonucleotide probe.

Fertility Analysis

To analyze male fertility, several independent pairs of fish were placed in the same tank for 1 week. Each pair consisted of a single male of the genotype of interest at two different age groups and a single young wild-type female (2 month old). On the seventh day, fertilized eggs were collected and counted. Unfertilized eggs die shortly after egg-laying and the yolk becomes opaque, allowing easy identification of fertilized versus unfertilized eggs. Results were expressed as a ratio of fertilized eggs per week of egg-lay.

Histology

Tissues samples were processed according to Harel et al. (2012). Briefly, tissues were fixed for 24h in Bouin's solution and paraffin-embedded. Sections of 4μm were stained with hematoxylin and eosin and examined by microscopy.

Blood Counts

Blood was drawn from adult male fish (n ≥ 3) according to Pedroso et al. (2012), collected into EDTA-coated tubes (BD) and sent for complete blood count on the same day (Animal Diagnostic Lab, Stanford).
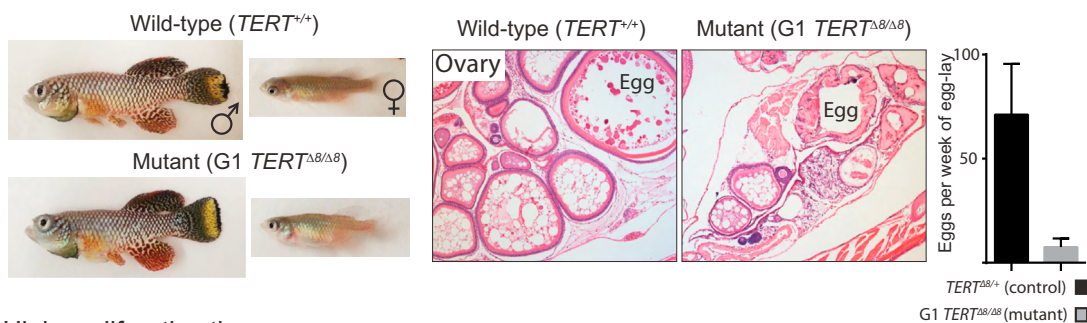
SUPPLEMENTAL REFERENCES

Feng, J., Liu, T., Qin, B., Zhang, Y., and Liu, X.S. (2012). Identifying ChIP-seq enrichment using MACS. Nat. Protoc. *7*, 1728–1740.

Gagnon, J.A., Valen, E., Thyme, S.B., Huang, P., Ahkmetova, L., Pauli, A., Montague, T.G., Zimmerman, S., Richter, C., and Schier, A.F. (2014). Efficient mutagenesis by Cas9 protein-mediated oligonucleotide insertion and large-scale assessment of single-guide RNAs. PLoS ONE *9*, e98186.

Harel, I., Maezawa, Y., Avraham, R., Rinon, A., Ma, H.Y., Cross, J.W., Leviatan, N., Hegesh, J., Roy, A., Jacob-Hirsch, J., et al. (2012). Pharyngeal mesoderm regulatory network controls cardiac and head muscle morphogenesis. Proc. Natl. Acad. Sci. USA *109*, 18839–18844.

Holt, C., and Yandell, M. (2011). MAKER2: an annotation pipeline and genome-database management tool for second-generation genome projects. BMC Bioinformatics *12*, 491.

Langmead, B., Trapnell, C., Pop, M., and Salzberg, S.L. (2009). Ultrafast and memory-efficient alignment of short DNA sequences to the human genome. Genome Biol. *10*, R25.

Pedroso, G.L., Hammes, T.O., Escobar, T.D., Fracasso, L.B., Forgiarini, L.F., and da Silveira, T.R. (2012). Blood collection for biochemical analysis in adult zebrafish. J. Vis. Exp. *63*, e3865.

Petzold, A., Reichwald, K., Groth, M., Taudien, S., Hartmann, N., Priebe, S., Shagin, D., Englert, C., and Platzer, M. (2013). The transcript catalogue of the short-lived fish *Nothobranchius furzeri* provides insights into age-dependent changes of mRNA levels. BMC Genomics *14*, 185.

Tamura, K., Stecher, G., Peterson, D., Filipski, A., and Kumar, S. (2013). MEGA6: Molecular Evolutionary Genetics Analysis version 6.0. Mol. Biol. Evol. *30*, 2725–2729.

Trapnell, C., Roberts, A., Goff, L., Pertea, G., Kim, D., Kelley, D.R., Pimentel, H., Salzberg, S.L., Rinn, J.L., and Pachter, L. (2012). Differential gene and transcript expression analysis of RNA-seq experiments with TopHat and Cufflinks. Nat. Protoc. *7*, 562–578.

Zhong, F.L., Batista, L.F., Freund, A., Pech, M.F., Venteicher, A.S., and Artandi, S.E. (2012). TPP1 OB-fold domain controls telomere maintenance by recruiting telomerase to chromosome ends. Cell *150*, 481–494.
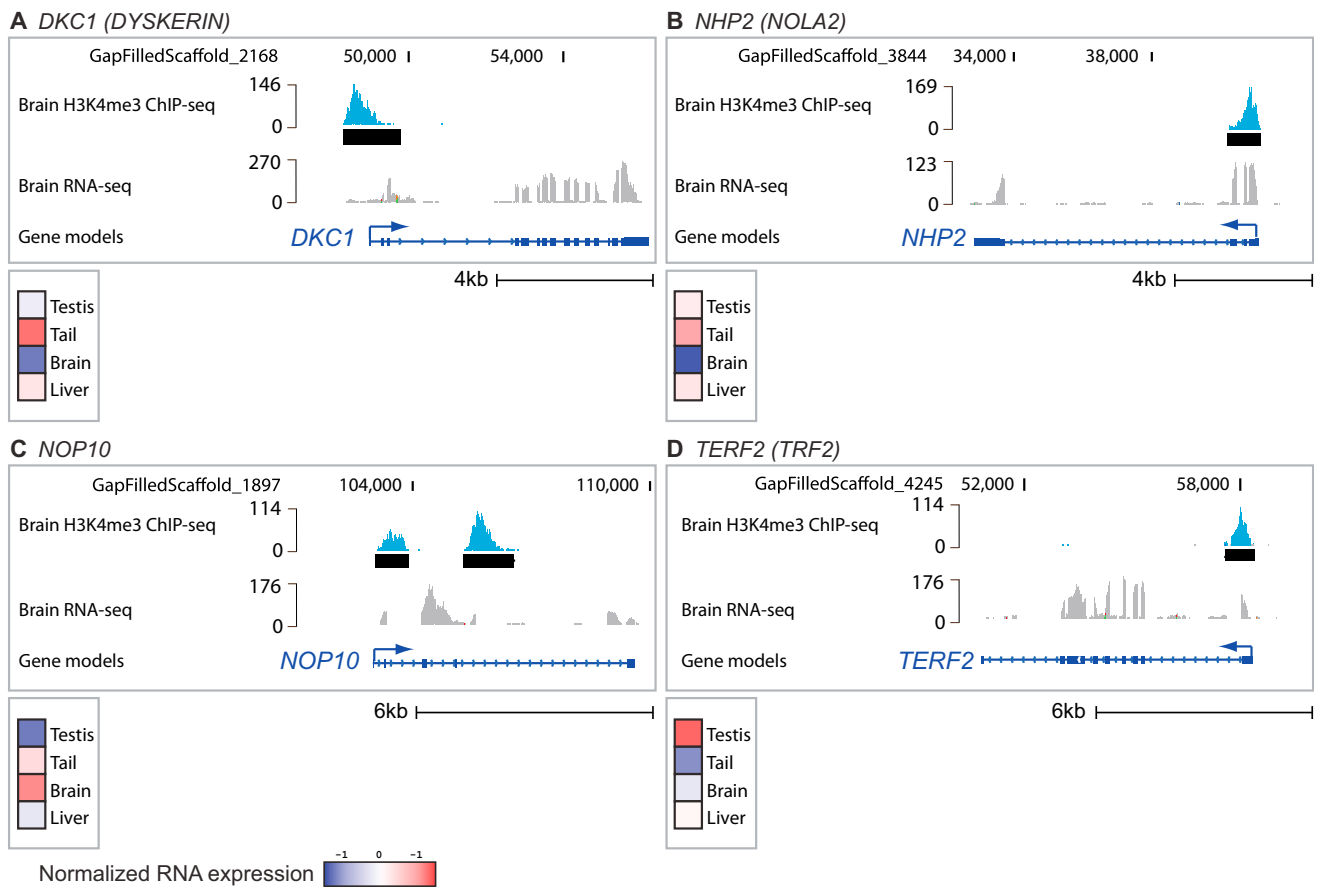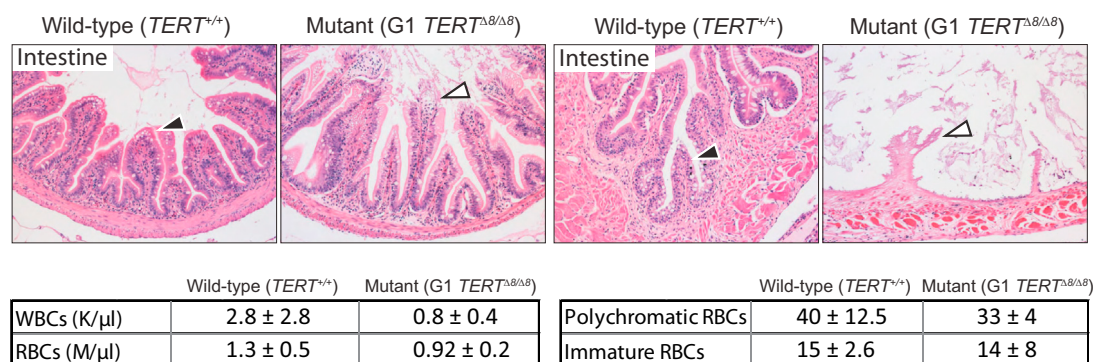
Figure S1. Genes Involved in Telomere Maintenance and Protection, Related to Figure 2
(A–D) Detailed genomic, epigenomic, and expression information for selected members of the TERT-associated proteins and shelterin complex.
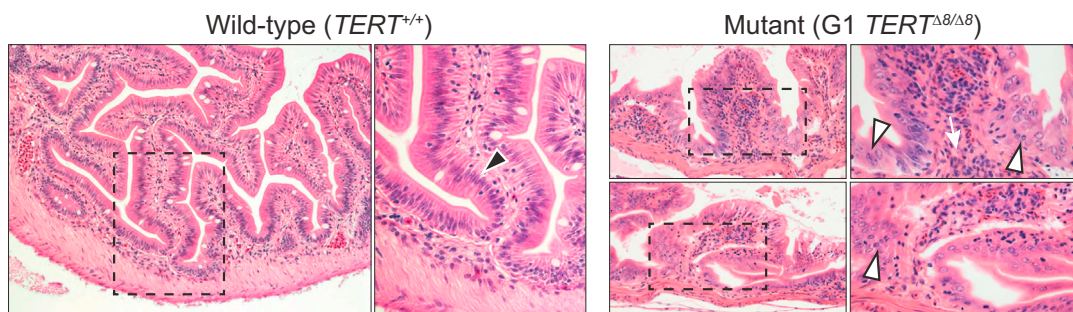
A 4-5 month old male & female fish

Wild-type (*TERT*⁺/⁺)

Mutant (G1 *TERT*^(Δ8/Δ8))

B Ovaries of 4-5 month old female fish

Wild-type (*TERT*⁺/⁺)   Mutant (G1 *TERT*^(Δ8/Δ8))

Ovary   Egg

Egg

TERT^(Δ8/+) (control) ■
G1 TERT^(Δ8/Δ8) (mutant) ▨

C High-proliferative tissues

Wild-type (*TERT*⁺/⁺)   Mutant (G1 *TERT*^(Δ8/Δ8))   Wild-type (*TERT*⁺/⁺)   Mutant (G1 *TERT*^(Δ8/Δ8))

Intestine   Intestine

	Wild-type (*TERT*⁺/⁺)	Mutant (G1 *TERT*^(Δ8/Δ8))
WBCs (K/µl)	2.8 ± 2.8	0.8 ± 0.4
RBCs (M/µl)	1.3 ± 0.5	0.92 ± 0.2

	Wild-type (*TERT*⁺/⁺)	Mutant (G1 *TERT*^(Δ8/Δ8))
Polychromatic RBCs	40 ± 12.5	33 ± 4
Immature RBCs	15 ± 2.6	14 ± 8

D Adenomatous changes in the intestine of mutant fish

Wild-type (*TERT*⁺/⁺)   Mutant (G1 *TERT*^(Δ8/Δ8))

E Low-proliferative tissues

Wild-type (*TERT*⁺/⁺)   Mutant (G1 *TERT*^(Δ8/Δ8))   Wild-type (*TERT*⁺/⁺)   Mutant (G1 *TERT*^(Δ8/Δ8))

Heart   Liver

Muscle   Kidney
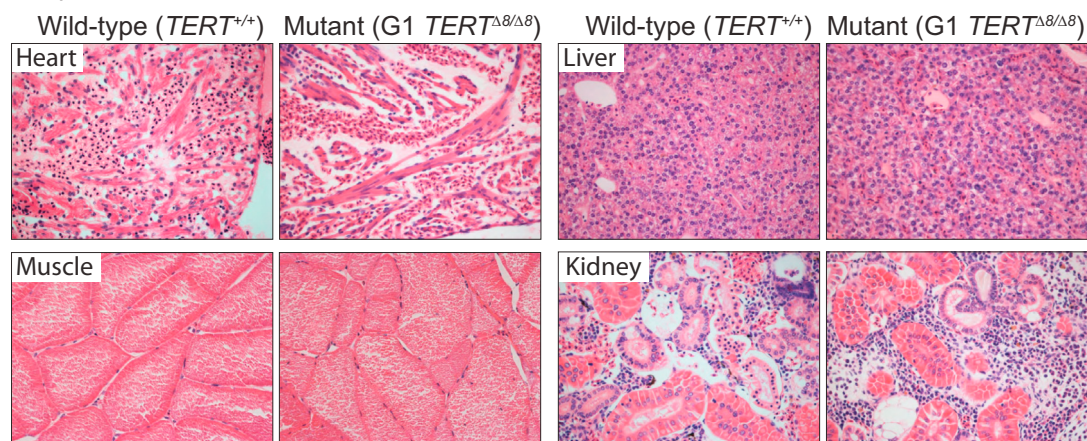
(legend on next page)

Figure S2. Histological Characterization of TERT-Deficient Turquoise Killifish, Related to Figure 3

(A) $TERT^{+/+}$ controls and G1 $TERT^{\Delta 8/\Delta 8}$ mutants are outwardly normal at 4-5 months of age.

(B) Histological characterization of ovaries from $TERT^{+/+}$ controls and G1 $TERT^{\Delta 8/\Delta 8}$ mutants (left panel). Total number of eggs per week of egg-lay for the indicated genotypes (right panel). Mean + SD of n ≥ 4 female for each genotype ($TERT^{+/+}$ versus G1 $TERT^{\Delta 8/\Delta 8}$).

(C) Histological characterization of high-proliferative tissues (gut, blood) in $TERT^{+/+}$ controls and G1 $TERT^{\Delta 8/\Delta 8}$ mutants. Blood cell count is mean ± SD of n ≥ 3 male for each genotype. RBC: red blood cell, WBC: white blood cell.

(D) Histological characterization of low-proliferative tissues (heart, muscle, liver, kidney) in $TERT^{+/+}$ controls and G1 $TERT^{\Delta 8/\Delta 8}$ mutants.

(E) Normal intestinal epithelia in wild-type fish (left panel, black arrowhead). Adenomatous changes in the intestine of G1 $TERT^{\Delta 8/\Delta 8}$ mutant fish (right panel, white arrowheads), as well as infiltration of inflammatory cells into the *lamina propria* (white arrow). Images for all tissues are from older males (4-5 months of age, n = 7), except for the ovaries which are from older females (4-5 months of age, n = 3).
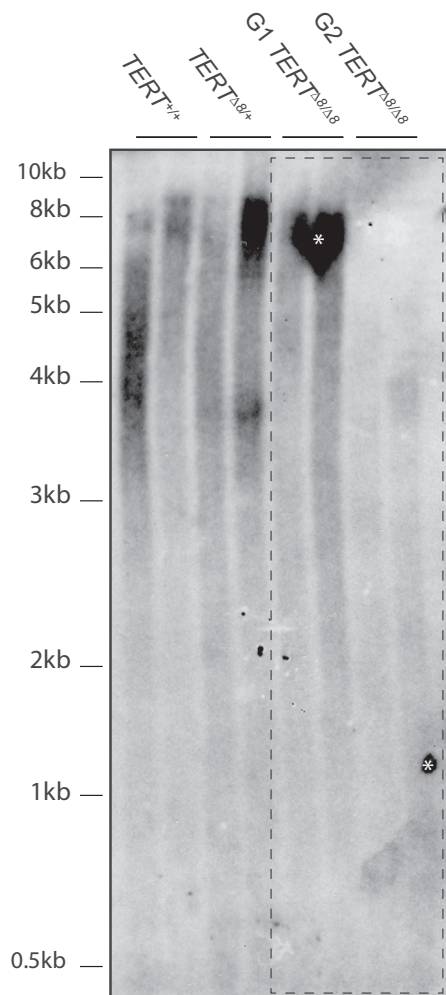
Figure S3. Telomere Length Measurement, Related to Figure 4

Telomere length measurement in embryos with the depicted genotypes, using the TRF Southern-blotting assay. A subset of this figure (dashed line) is presented in Figure 4D. White asterisk: non-specific probe binding.
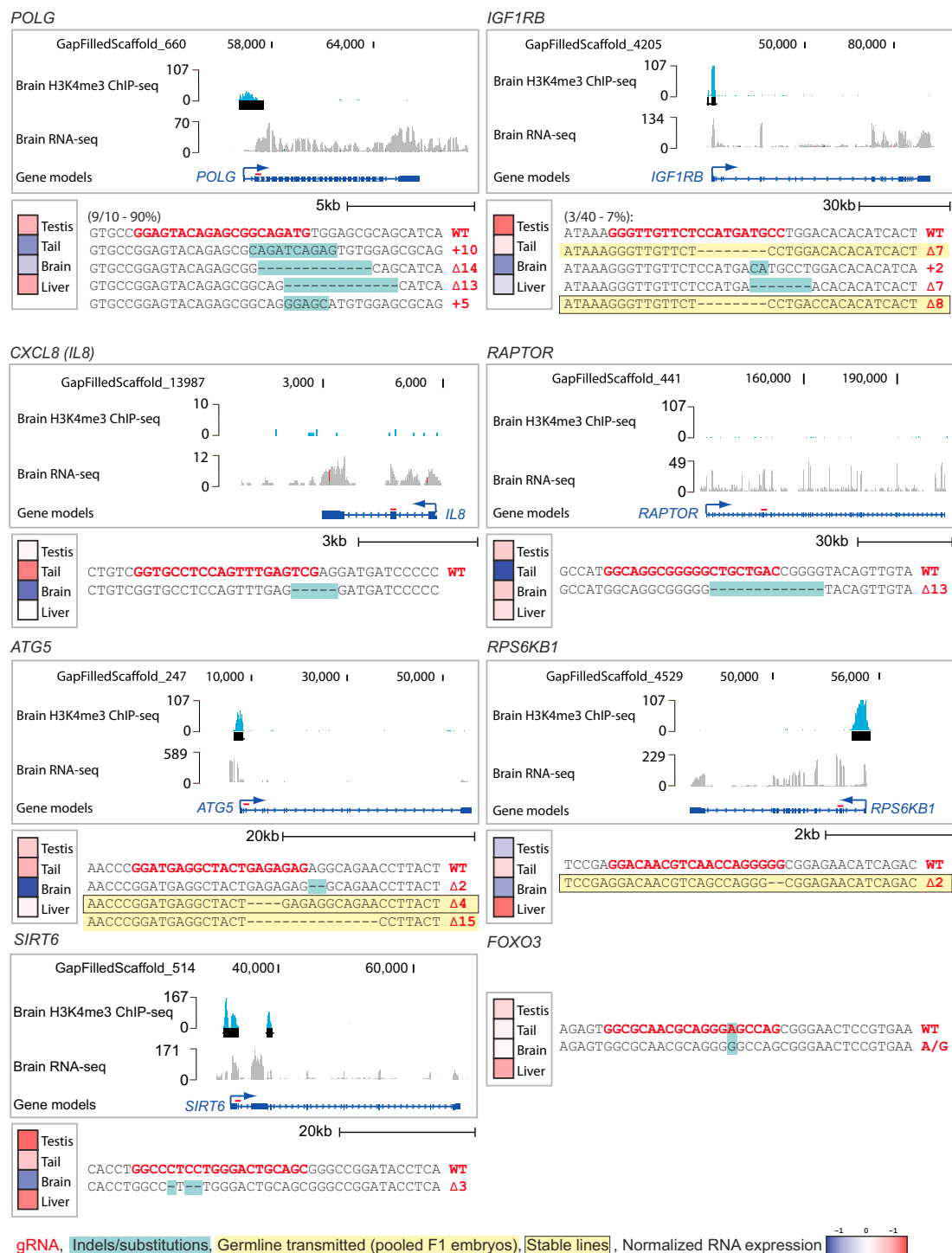
Figure S4. Additional Targeted Genes, Related to Figures 5 and 6

Detailed genomic, epigenomic, expression information, and range of detected indels for additional targeted genes. *FOXO3* does not have a complete gene model because the gene has a very long second intron (as in mammals) and is therefore split between two genomic scaffolds. For *IGF1RB*, the Δ8 stable line was generated by a separate pair of founders and therefore was not part of the efficiency calculation.